# Gamma decay of high spin states in $^{25}$Mg above 6.1 MeV

D. M. Headly* and R. K. Sheline
*Department of Chemistry, Florida State University, Tallahassee, Florida 32306*

S. L. Tabor, U. J. Hüttmeier,† C. J. Gross,‡ and E. F. Moore§
*Department of Physics, Florida State University, Tallahassee, Florida 32306*

B. H. Wildenthal**
*Department of Physics and Atmospheric Sciences, Drexel University, Philadelphia, Pennsylvania 19104*

H. R. Weller and R. M. Whitton
*Duke University and Triangle Universities Nuclear Laboratory, Durham, North Carolina 27706*

I. Ragnarsson
*Department of Mathematical Physics, Lund Institute of Technology, S-221 00 Lund, Sweden*
(Received 24 February 1988)

New high spin states in $^{25}$Mg (up to 13.3 MeV in excitation) have been located using the $^{12}$C($^{14}$N,$p\gamma$)$^{25}$Mg reaction at a laboratory beam energy of 23.5 MeV. Gamma decay from 28 neutron unbound levels has been observed (24 of which are reported here for the first time) up to 7 MeV above the neutron drip line. Tentative identification of the yrast line up to $\frac{17}{2}^+$ has been made, along with an extension of the ground-state rotational band up to $\frac{15}{2}^+$ and the location of several other states with $J^\pi=\frac{11}{2}^+$ and $\frac{15}{2}^+$. Extensive comparison with the *s-d* shell model and the cranked Nilsson-Strutinsky model has been made for the states in $^{25}$Mg. Very good agreement is observed between the shell model and experimental level energies and $\gamma$-decay branches. Potential energy surfaces for $J^\pi=\frac{11}{2}^+$, $\frac{13}{2}^+$, and $\frac{17}{2}^+$ in the cranked Nilsson-Strutinsky model show a noncollective oblate local minimum at $(\epsilon_2,\gamma)=(0.34,60°)$ for $\frac{11}{2}^+$ and prolate configurations at $(0.2,-120°)$ for $\frac{13}{2}^+$ and $\frac{17}{2}^+$. These states compete with the collective ground-state band members at $\gamma\approx 0°$ and become yrast for $\frac{17}{2}^+$. The stabilization of these prolate aligned states relative to more deformed, collective states of the same spin results from shell effects at high spin in the cranking model, and provides a description of the configuration in the yrast $8^+$; $\frac{11}{2}^+$, $\frac{13}{2}^+$, and $\frac{17}{2}^+$; and $4^+$ states in $^{24}$Mg, $^{25}$Mg, and $^{26}$Mg, respectively.

## I. INTRODUCTION

$^{25}$Mg was one of the earliest and best examples of quadrupole-deformed nuclei in the $A=19-28$ mass region. The interpretation of the low-lying excitation region in $^{25}$Mg, exhibiting the rotational spectrum of a prolate deformed system, was first made by Litherland *et al.* in 1958[1] using the collective model of Nilsson.[2] The excitation spectrum of this nucleus below 6.1 MeV has been studied in the intervening years, and spins up to $\frac{13}{2}^+$ have been observed.[3–9] A 1978 review of the $^{25}$Mg literature by Endt and Van der Leun[10] recommended additional experimental study. This research attempts to answer some of the experimental and theoretical problems in $^{25}$Mg spectroscopy. Preliminary results have already been reported.[11]

With the recent use of the cranking model in interpreting nuclear spectra and the success of the *s-d* shell model using the full basis space in reproducing energies and decay properties in this mass region, it becomes more important to investigate the level scheme of $^{25}$Mg at higher spins. This nucleus provides us with an opportunity to compare the predictions of the purely microscopic shell model (SM) with the cranked Nilsson model including Strutinsky renormalization (CNSM), and in particular to extend the latter's concept of coexisting prolate shapes in $^{24}$Mg due to rotation about two different axes[12,13] to other nuclei.

To emphasize high-spin states this work is the first detailed investigation of $^{25}$Mg using heavy-ion beams. High-spin states up to 13.3 MeV in excitation have been selectively populated using the reaction $^{12}$C($^{14}$N,$p\gamma$)$^{25}$Mg at 23.5 MeV. The contour diagram of Fig. 1 illustrates this high-spin selectivity, where $l^{\rm in}_{\rm graz}$ and $l^{\rm out}_{\rm graz}$ represent the coupled incident and outgoing grazing angular momenta.[14] Here "grazing" means the value of $l$ where $T_l$, the transmission coefficient for that partial wave, is $\frac{1}{2}$. Using optical-model parameters for known discrete states in $^{25}$Mg (Ref. 15) and a Hauser-Feshbach calculation of $T_l$ values in the entrance and exit channels, the results shown in Fig. 1 suggest strong selectivity since the overlap of experimental levels with the area between $l^{\rm in}_{\rm graz}$ and $l^{\rm out}_{\rm graz}$ is small.

The present investigation was focused on states in $^{25}$Mg

 

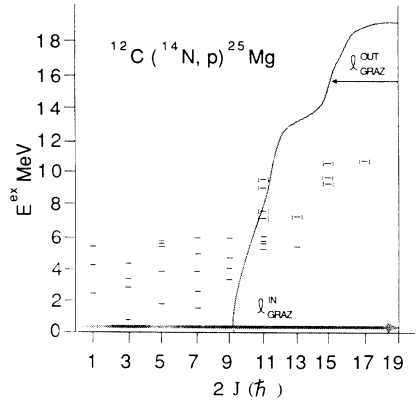


FIG. 1. Test of high-spin selectivity using an angular momentum mismatch formalism for the reaction $^{12}$C($^{14}$N,$p$)$^{25}$Mg at 23.5 MeV. The values of $l^{\text{in}}_{\text{graz}}$ and $l^{\text{out}}_{\text{graz}}$ were calculated using Hauser-Feshbach estimates of transmission coefficients. Selectivity is expected for yrast or near-yrast states lying inside the intersection of $l^{\text{in}}_{\text{graz}}$ and $l^{\text{out}}_{\text{graz}}$.

above 7.4 MeV, where new high-spin states are most likely to be found. The neutron binding energy is 7.332 MeV so that neutron decay competes strongly with $\gamma$ decay above the threshold. In fact, the open neutron channel with its angular momentum barrier provides a high-spin selective filter permitting only the $\gamma$ decays of high-spin states to be observed.

## II. EXPERIMENTAL METHODS

In order to find the most favorable beam energy, an excitation function was measured for the $^{12}$C($^{14}$N,$p$)$^{25}$Mg reaction between 19 and 26.5 MeV, in steps of 0.25 MeV. The $^{14}$N beam was produced by the Florida State University FN tandem accelerator. Beam currents for all the experiments performed ranged from 50 to 190 nA. From the excitation curve, 23.5 MeV was selected as the energy that most strongly and cleanly populated higher-spin states ($J \geq \frac{9}{2}$) in $^{25}$Mg. All subsequent experiments were performed at this energy.

Proton-$\gamma$ coincidences were measured between an $E$[4 mm Si(Li) $-\Delta E$ [75 $\mu$m Si] telescope arrangement at 0° to the beam and either of two Ge(Li) detectors placed at 90°. The particle telescope subtended a solid angle of 76 msr, and the Ge(Li) detector efficiencies were 16 and 25%. A 50-$\mu$g/cm$^2$-$^{12}$C target was made by evaporation onto a 12.5-$\mu$m-thick $^{58}$Ni foil. The bulk of the $\gamma$-$\gamma$ coincidence data was measured at the Triangle Universities Nuclear Laboratory. Two 25% efficient Ge detectors were placed at 90° to the beam direction on either side of the target.

Proton-$\gamma$ angular correlations were measured to identify the spins of new states. Particles were again measured at 0° (76 msr telescope solid angle) while the $\gamma$ rays were detected at 90°, 81°, 120°, and 158°. Relative efficiencies for the $\gamma$ detectors ranged from 25% to 11%. Two self-supporting $^{12}$C targets were used for this experiment with thicknesses in the range of 60–140 $\mu$g/cm$^2$. A $^{58}$Ni foil was placed behind the targets on a separate frame, with a resulting gap between target and foil of roughly 1.4 mm. This arrangement allowed full Doppler shifting of $\gamma$ rays. Targets were switched once during the 11-day run to compensate for $^{12}$C buildup which continually degraded particle resolution. The resultant FWHM for proton peaks was $\leq$400 keV (see Fig. 2).

The angular correlations were measured using the "method II" geometry of Litherland and Ferguson.[16] Detection of the protons at 0° limited the possible magnetic substates populated in $^{25}$Mg to $\pm\frac{1}{2}$ and $\pm\frac{3}{2}$. Finite-geometry effects were not large. The maximum particle telescope half-angle about the beam axis was 10°, while statistical model calculations predict the maximum angular momentum carried away by the proton in this experiment to be $4\hbar$. Classically then, $l_z$(proton) $\leq 0.7\hbar$ ($Z$ is along the beam axis), so that no $m_z = \pm\frac{5}{2}$ substates would be populated in $^{25}$Mg. Other analyses of similar geometries and ejectile angular momenta[16–18] have estimated the contribution of $\pm\frac{5}{2}$ substates to be no more than a few percent of the $P_2$ term in the angular distribution:

$$I(\theta) = 1 + a_2 P_2 \cos\theta + a_4 P_4 \cos\theta \,, \tag{1}$$

where $I(\theta)$ is the intensity at an angle $\theta$ between the detected $\gamma$ ray and the beam axis.

The $a_k$ coefficients in Eq. (1) are given by

$$a_k = Q_k j_1 [P(-1)^{J_1 - 1/2} C(J_1 J_1 K; \tfrac{1}{2} - \tfrac{1}{2}\, 0) + (1-P)(-)^{J_1 - 3/2} C(J_1 J_1 K; \tfrac{3}{2} - \tfrac{3}{2}\, 0)]$$
$$\times [R_k(l_0 l_0 J_1 J_1) + 2R_k(l_0 l J_1 J_1)\delta + R_k(l l J_1 J_1)\delta^2]/(1+\delta^2) \tag{2}$$

for a transition from $J_1$ to $J_2$ and $m_1 = \pm\frac{1}{2}, \pm\frac{3}{2}$.[18] The $Q_K$ are standard, finite solid-angle-detector attenuation coefficients and $l_0$ and $l$ are the lowest- and next-lowest-allowed multipolarities, with $l_0 = |J_1 - J_2|$. The population parameter for $m_1$ substates,

$$P = 2W(\tfrac{1}{2}), \quad W(\tfrac{1}{2}) + W(\tfrac{3}{2}) = \tfrac{1}{2} \tag{3}$$

and the mixing ratio,

$$\delta = \frac{\langle J_1 \| T^{\pi}_{L} \| J_2 \rangle}{\langle J_1 \| T^{\pi_0}_{L_0} \| J_2 \rangle} \frac{\hat{L}_0}{\hat{L}}, \quad \delta_{L_0} = 1 \tag{4}$$

along with $J_1$ and $J_2$ are the variables in Eq. (1). The convention for $\delta$ is the same as that of Rose and Brink.[19] Assuming a specific $J_1, J_2$ pair, theoretical angular distributions were calculated using (1), (2), and a specific $P$ and $\delta$. Only three data points were used; the small 90° detector proved too inefficient at detecting the weak transi-

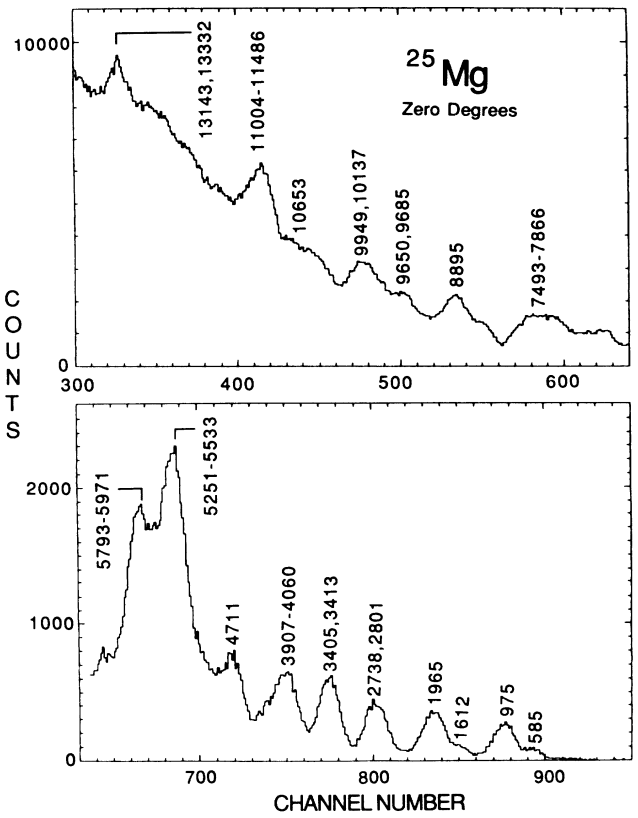


FIG. 2. A representative spectrum of total protons collected in a 0° telescope using the $^{12}C(^{14}N,p)^{25}Mg$ reaction at 23.5 MeV. Energies in keV above specific peaks represent the excitation energy of states in $^{25}Mg$; if more than one state makes up a peak the energies represent the state or range of states (indicated by a dash) contributing the majority of counts.

tions from unbound states. A standard $\chi^2$ analysis (one degree of freedom) was then performed for $\tan^{-1}(\delta) = -90°$ to $+90°$ and variable $P$. It was found that for values of $P > 0.5$ the effect on the position of minima in $\chi^2$ versus $\delta$ was small, as seen in other work,[20] and a value of 0.8 for $P$ was used for all analyses. A combination of $J_1$, $J_2$, and $\delta$ values was considered acceptable if $\chi^2$ dropped below 10.8, the 0.1% confidence level. Errors in $\delta$ at minima in $\chi^2$ were taken from the intersection of the curve with the larger of two values: $\chi^2 = 1$ or $1.5\chi^2$(min).

Energies of $\gamma$ rays were calculated assuming full Doppler shifts. Branching ratios were determined by summing over the three angles weighted by $\sin\theta$. Single-escape (SE) and double-escape (DE) peaks were not included when calculating branching ratios since they were not included in the efficiency calibrations. As labeled in Table II, many branching ratios are derived from transitions observed only at 158°, where the most efficient detector was located and where the $E2$ angular distributions are stronger.

Further information on the spins and parities of the new high-lying states comes from the successful competition of the observed $\gamma$ transitions with neutron decay. Basically only the fastest $\gamma$ decays ($E2$, $M1+E2$, or $E1+M2$) can compete and then only if neutron decay is inhibited by a substantial angular momentum barrier. More precisely, for a given spin-parity hypothesis for a particular initial state, we have estimated the minimum total $\gamma$-decay strength which could compete by assuming it must equal the neutron-decay strength. The neutron-decay width was calculated with a barrier penetration program and conservatively multiplied by 0.01 as a typical minimum spectroscopic strength. The acceptability of the spin-parity hypothesis was determined by comparison of the minimum $\gamma$-decay strength in each observed branch with the upper limits suggested by Endt and Van der Leun[10] for $A = 21-44$ nuclei—0.03 Weisskopf units (W.u.) for $E1$ radiation, 10 W.u. for $M1$, 100 W.u. for $E2$ and 3 W.u. for $M2$ radiation. A comparison with SM and CNSM predictions was also helpful in assigning tentative spins.

## III. EXPERIMENTAL RESULTS

### A. Level scheme and branching ratios

Figure 2 displays a 0° proton spectrum in coincidence with all $\gamma$ rays at 90°. The relatively large peak containing the $\frac{13}{2}_1^+$ and $\frac{11}{2}_{1,2}^+$ states around an excitation energy of 5.5 MeV demonstrates the selective population involved at 23.5 MeV beam energy. Figure 3 displays protons in coincidence with only the yrast $\frac{13}{2}^+ \rightarrow \frac{9}{2}^+$ transition in $^{25}Mg$ from the angular correlation experiment. Projecting out proton peaks gated by $\gamma$ rays in this manner supplemented the determination of level energies by the reverse procedure. This is shown in Fig. 4 for $\gamma$ rays gated by the 9.48–10.4 MeV excitation region. Very little confirmation of new $\gamma$ transitions was obtained from $\gamma$-$\gamma$ coincidence measurements. This was mainly due to the inability to uniquely select excitation energies in $^{25}Mg$ as is done with proton detection.

The analysis of coincidence spectra has produced the

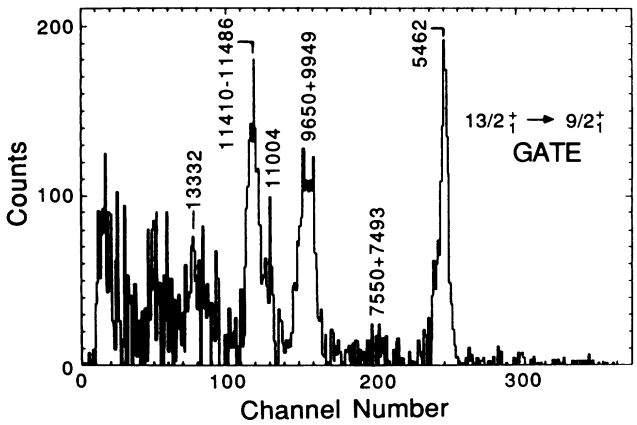


FIG. 3. A summed proton spectrum in coincidence with $\gamma$ rays at four angles in the angular correlation experiment from the $\frac{13}{2}_1^+ \rightarrow \frac{9}{2}_1^+$ transition in $^{25}Mg$. Numbers refer to the excitation energy in keV of states in $^{25}Mg$.

level scheme shown in Fig. 5 and the branching ratios in Tables I and II. In Fig. 5 only decays from states above 6.1 MeV are shown. As listed in Table II, several new levels were determined by assuming full Doppler shifting of $\gamma$ rays observed only at 158° in the angular correlation run. Particle resolution was about 300 keV in the coincidence measurements because of the need to keep counting rates high. Many new weak $\gamma$ rays could not be placed in the level scheme due to limited statistics and the existence of several possible final states within 300 keV. The yrast $\frac{13}{2}^+ \rightarrow \frac{9}{2}^+ \rightarrow \frac{7}{2}^+ \rightarrow \frac{5}{2}^+$ $\gamma$-ray cascade was observed in spectra gated by excitation energies up to 14.5 MeV. However, the competing $^{24}$Mg $\gamma$ decay was much stronger in the high-excitation regions. The resulting Compton background virtually eliminated any change of seeing weak successive $\gamma$-ray cascades to known states from the 14-MeV region, as well as from the states at 13.143 and 13.332 MeV and to a lesser extent from the 11.4-MeV cluster of states.

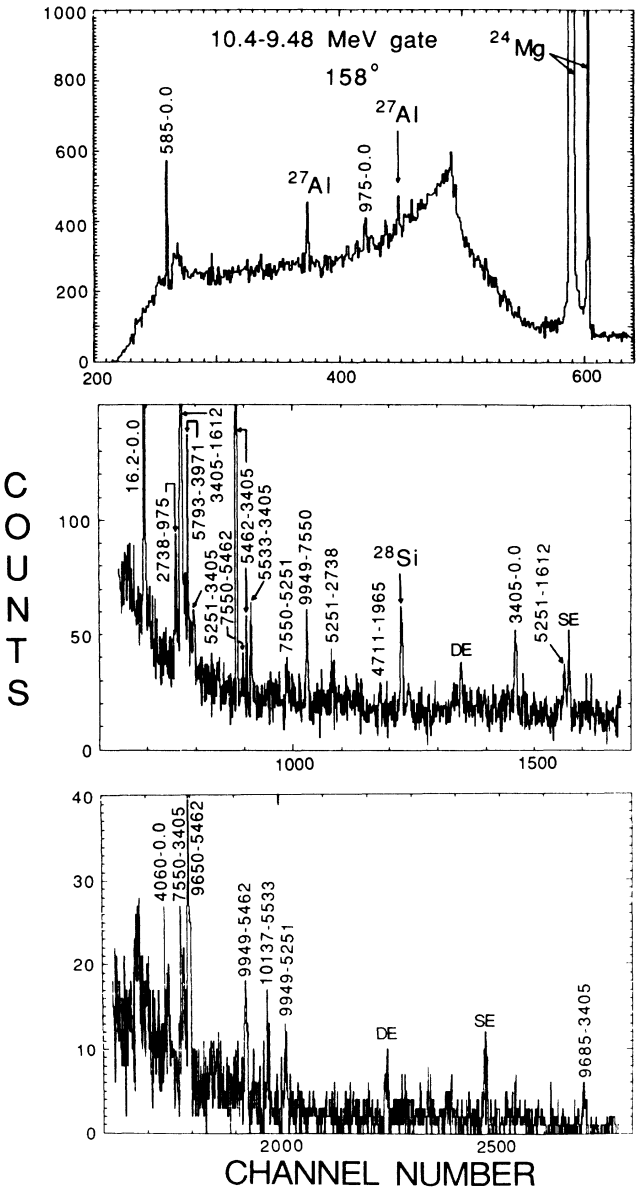


FIG. 4. $\gamma$-ray spectrum at 158° in coincidence with the 10.4–9.48 MeV excitation energy ration in $^{25}$Mg. Transitions in $^{25}$Mg are labeled by the initial and final energies, and SE and DE refer to the single- and double-escape peaks of $\gamma$ rays to their right. Contaminant peaks are labeled by nucleus.

Table I summarizes the previously known $\gamma$-ray transitions for states below 6.1 MeV, where enough statistics were available in the present work to calculate branching and/or mixing ratios. A comparison between present and earlier work helps to evaluate the degree of confidence that we can have for new levels using only three angles and limited statistics for most transitions. The branching ratios agree within one standard deviation for 6 of 17 transitions from states with more than one branch and within 5% for 9 of the remaining 11.

In Table II properties of the states above 6.1 MeV are listed along with results from Röpke *et al.*[5] Present level energies are 12±3 keV above the earlier values. The analog-to-digital converters (ADC's) used in this work were very linear with $\gamma$-ray energy, and comparing previously known $\gamma$-ray energies observed here with literature values supports the present level energies in Table II. The fact that only the strongest transitions observed from Röpke's work (populated with a deuteron beam) were observed here strongly suggests that the 13 states seen in both experiments are of medium or low spin. The previously observed branches were used in determining ranges of possible spins in this work.

### B. Angular correlations and spin assignments

The results of the present mixing-ratio calculations are given in Tables I and III, along with previous results. Seventeen of the 25 values for $\delta$ in Table I agree within uncertainty with earlier work. However, for almost every transition fitted with $J_f - 2 \leq J_i \leq J_f + 2$, more than one $J_i$ value was allowed at the 0.1% confidence level, a general ambiguity which has been discussed in detail by Twin.[21] Graphs of $\chi^2$ versus $\delta$ are shown in Fig. 6 for the yrast $\frac{9}{2}^+ \rightarrow \frac{7}{2}^+$ and $\frac{7}{2}^+ \rightarrow \frac{5}{2}^+$ transitions. The convention used for all such plots is that $J_f$ is fixed to its known value, and the various curves correspond to different $J_i$ values. The minima in $\chi^2$ closer to $\delta = 0$ for the correct $J_i$ value in both transitions reproduce earlier work.

The Legendre polynomial coefficients in Tables I and III were obtained from minima in $\chi^2$ and not by fitting a curve to the data since only three angle points were measured. Analysis of specific states and their spin assignments will now be made, using the neutron barrier estimates discussed above.

### C. Discussion of individual states

To facilitate this discussion, previously known and newly assigned states in $^{25}$Mg are listed in Table IV along with their spin assignments. The theoretical interpretations in terms of rotational bands or shell-model configurations are also given.

### 1. Levels below 6.1 MeV

The states at 5251, 5793, and 6041 keV have previously been assigned tentative spins of $\frac{11}{2}^+$, $\frac{11}{2}^-$, and $\frac{11}{2}^+$, respectively, with the $\frac{7}{2}$ possibility for each case not ruled out.[6–8,10] The 6041-keV state was not populated as strongly as other high-spin states were in this work, and no new states have been identified as decaying to this level, although the 6041–3405-keV transition was seen in coincidence with excitation regions between 7 and 11.5 MeV. No new information on the spin of this state could be determined from the present work.

A spin of $\frac{7}{2}^{\pm}$ could not be ruled out for the states at 5251 and 5793 keV from the present angular correlations. However, decay information from higher levels shows almost certainly that these states have $J=\frac{11}{2}$ as will be discussed in Secs. III C 2 and V.

### 2. Levels above 6.1 MeV

The 7501-keV state will be used as an example of the information provided by neutron partial widths. Decays to states with $J^\pi=\frac{7}{2}_2^+$, $\frac{3}{2}_1^+$ and $\frac{5}{2}_1^+$ restrict $J_i^\pi$ to $\frac{3}{2}^+$, $\frac{5}{2}^{\pm}$, or $\frac{7}{2}^+$. The possibility $J_i^\pi=\frac{3}{2}^+$ can be ruled out because the neutron decay to the ground state of $^{24}$Mg would

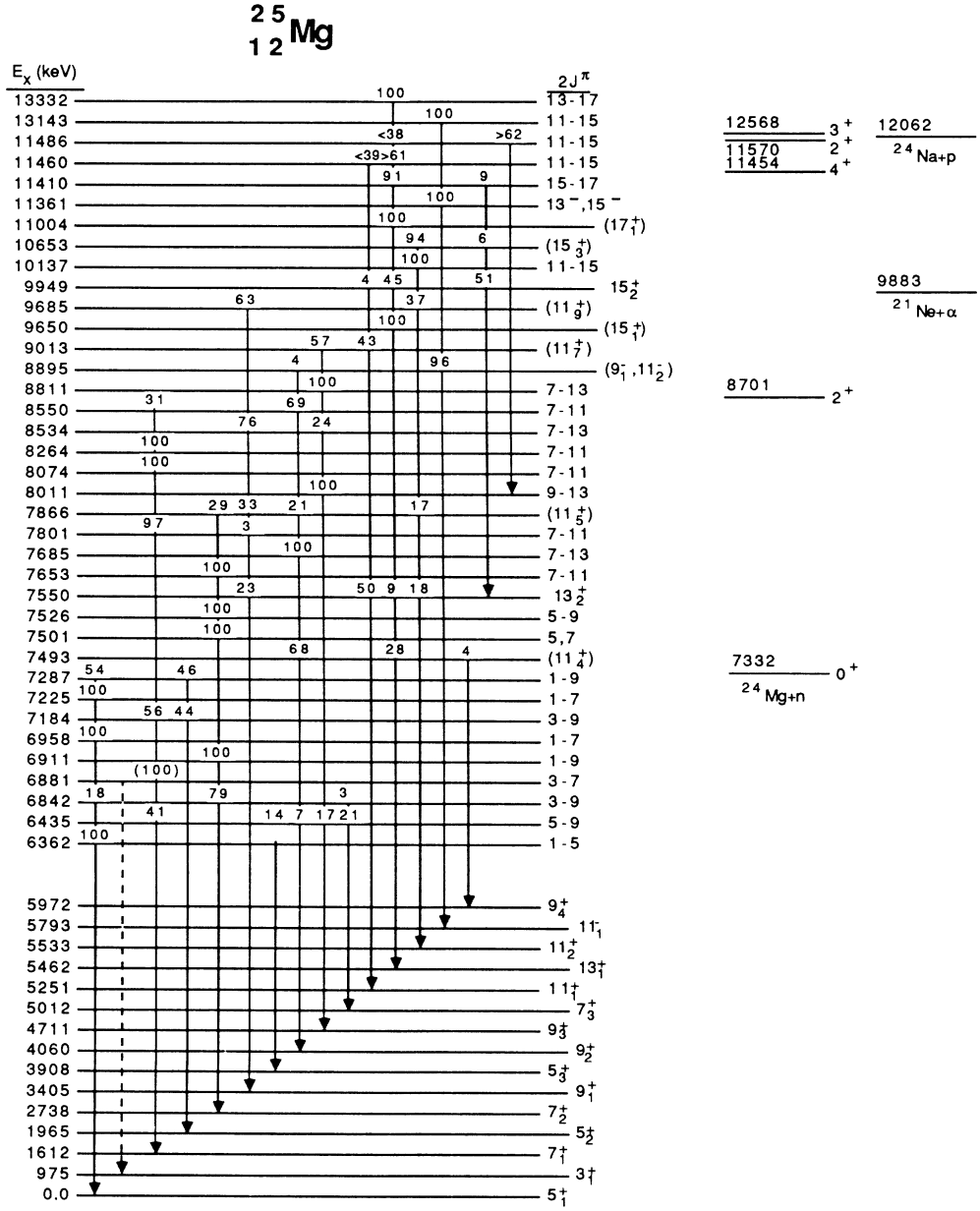


FIG. 5. Gamma-decay scheme for $^{25}$Mg levels above 6 MeV in excitation energy from the present work. The spin(s) for each level is given as $2J$. Parentheses around spins of particular states signify a tentative assignment based on comparison of experiment and theory. The positions of levels accessible to particle decay are also shown. Branching ratios are listed above the initial state.

occur with a width of at least 70 eV, assuming a spectroscopic factor $\geq 0.01$. A comparable total $\gamma$ decay width at 70 eV would imply an $E2$ strength of 3000 W.u. for the 38% branch to the $\frac{7}{2}_2^+$ state. This is a factor of 30 larger than any known $E2$ strength in the *s-d* shell.

Figure 7 displays $\chi^2$ versus $\delta$ for the 7550–5251-keV transition. Assuming for the moment that $J(5251)=\frac{11}{2}$ decays to states with $J^\pi=9/2_1^+$, $\frac{11}{2}{}^+_{1,2}$, and $\frac{13}{2}{}^+_1$ restrict $J_i^\pi(7550)$ to $\frac{9}{2}^+$, $\frac{11}{2}^\pm$, or $\frac{13}{2}^+$. No spins in Fig. 7 can be ruled out at the 0.1% confidence level, although the $\frac{11}{2}$ candidate is less likely. The curve for $j_i=\frac{13}{2}$ gives a pos-

TABLE I. Summary of all previously known $\gamma$-ray transitions where decay information could be extracted in the present work. Included are branching ratios (BR), mixing ratios ($\delta$), and present Legendre polynomial coefficients corresponding to the minimum in $\chi^2$ vs $\delta$. Where available, shell model (SM) predictions are also compared. Unless otherwise indicated, all previous results come from Endt and Van der Leun (Ref. 10) and $\delta_{SM}(E2)=0.0$.

| | | | BR (%) | | | | | $\delta$ | | |
|---|---|---|---|---|---|---|---|---|---|---|
| $E_i-E_f$ (keV) | $J_i^\pi$ | $J_f^\pi$ | Present | Previous | SM | $A_2/A_0$ | $A_4/A_0$ | Present | Previous | SM |
| 1 965 – 0.0 | $\frac{5}{2}^+$ | $\frac{5}{2}^+$ | 25±3 | 26±1 | | −0.15 | −0.04 | 0.58±0.07 | 0.6±0.1 | |
| −585 | | $\frac{1}{2}^+$ | 50±3 | 47±1 | | 0.29 | −0.48 | 0.34±0.25 | 0.0 | |
| −975 | | $\frac{3}{2}^+$ | 25±3 | 27±1 | | −0.68 | 0.016 | 0.25±0.17 | 0.25±0.07 | |
| 1 612 – 0.0 | $\frac{7}{2}^+$ | $\frac{5}{2}^+$ | 100 | 100 | | −0.59 | 0.010 | 0.18±0.07 | 0.19±0.02 | |
| 2 801 – 585 | $\frac{3}{2}^+$ | $\frac{1}{2}^+$ | a | 39±2 | | −0.060 | 0.0 | −0.21±0.09 | $-11<\delta<2.3$[c] | |
| 3 405 – 0.0 | $\frac{9}{2}^+$ | $\frac{5}{2}^+$ | 25±3[b] | 19±1 | 28 | 0.058 | −0.024 | −0.14±0.09 | 0.0 | |
| −1612 | | $\frac{7}{2}^+$ | 75±3 | 81±1 | 72 | −0.052 | 0.01 | 0.12±0.02 | 0.14±0.02 | 0.14 |
| 4 060 – 0.0 | $\frac{9}{2}^+$ | $\frac{5}{2}^+$ | 55±4[b] | 60±1 | 5 | 0.34 | −0.32 | 0.09±0.05 | 0.0 | |
| −1612 | | $\frac{7}{2}^+$ | 45±4 | 39±1 | 94 | −1.8 | 0.10 | 0.53±0.12 | 0.46±0.10 | 0.26 |
| 4 711 – 1965 | $\frac{9}{2}^+$ | $\frac{5}{2}^+$ | a | 94±1 | 82 | 0.49 | −0.14 | −0.05±0.08 | −0.02±0.02[d] | |
| −1612 | | $\frac{7}{2}^+$ | | 0 | 7 | | | | | |
| −2738 | | $\frac{7}{2}^+$ | | 6±1 | 8 | | | | | |
| 4 722 – 975 | $\frac{5}{2}^+$ | $\frac{3}{2}^+$ | 100 | 100 | | −0.35 | 0.0 | 0.02±0.07 | $-0.27<\delta<-0.12$[c] | |
| | $\frac{3}{2}^-$ | $\frac{3}{2}^+$ | | | | −0.34 | 0.0 | 1.28±0.63 | $0.1<\delta<0.4$ | |
| 5 012 – 1965 | $\frac{7}{2}^+$ | $\frac{5}{2}^+$ | a | 42±1 | | −0.50 | 0.005 | 0.11±0.11 | 0.0±0.03 | |
| 5 251 – 4060 | $\frac{11}{2}^+$ | $\frac{9}{2}^+$ | 22±4 | 23±1 | 7 | −0.39 | 0.001 | 0.052±0.058 | 0.11±0.02[e] | 0.19 |
| −3405 | | $\frac{9}{2}^+$ | 19±3 | 28±2 | 57 | −0.027 | 0.009 | −0.14±0.09 | 0.04±0.02[e] | 0.12 |
| −2738 | | $\frac{7}{2}^+$ | 12±4 | 14±2 | 2 | | | f | 0.0 | |
| −1612 | | $\frac{7}{2}^+$ | 48±5[b] | 35±3 | 34 | 0.34 | −0.28 | 0.07±0.09 | 0.0 | |
| 5 462 – 3405 | $\frac{13}{2}^+$ | $\frac{9}{2}^+$ | 100 | 100 | 85 | 0.33 | −0.26 | 0.07±0.07 | −0.02±0.02[d] | |
| | | | | | (14→4060) | | | | | |
| 5 533 – 3405 | $\frac{11}{2}^+$ | $\frac{9}{2}^+$ | 71±4 | 61±3 | 69 | −0.52 | 0.01 | 0.12±0.06 | 0.03±0.03 | 0.13 |
| −1612 | | $\frac{7}{2}^+$ | 29±4 | 39±3 | 23 | | | f | | |
| | | | | | (4→4060) | | | | | |
| | | | | | (4→2738) | | | | | |
| 5 747 – 0.0 | $\frac{5}{2}^+$ | $\frac{5}{2}^+$ | a | 78±1 | | −0.18 | −0.044 | 0.62±0.11 | 0.40±0.11[e] | |
| | $\frac{3}{2}^+$ | $\frac{5}{2}^+$ | | | | −0.19 | 0.0 | −0.19±0.13 | 0.07±0.02[e] | |
| 5 793 – 3971 | $\frac{11}{2}^-$ | $\frac{7}{2}^-$ | 26±4 | 34±1 | | 0.40 | −0.21 | 0.02±0.08 | 0.0[b] | |
| −3405 | | $\frac{9}{2}^+$ | 74±4 | 66±1 | | −0.61 | 0.01 | 0.18±0.06 | 0.01±0.01[e] | |
| 5 971 – 4060 | $\frac{9}{2}^+$ | $\frac{9}{2}^+$ | 27±6 | 41±1 | | 0.54 | −0.03 | −0.27±0.54 | 0.0±0.07 | |
| −1612 | | $\frac{7}{2}^+$ | 73±6[b] | 51±1 | | −0.43 | 0.0 | 0.07±0.10 | 0.31±0.03 | |
| 6 041 – 3405 | $\frac{11}{2}^+$ | $\frac{9}{2}^+$ | a | 84±2 | 46 | −0.8 | 0.039 | $0.31\ ^{+0.24}_{-0.15}$ | 0.13±0.04 | 0.19 |
| | $\frac{7}{2}^+$ | $\frac{9}{2}^+$ | | | | −0.78 | 0.026 | $\delta<-0.31$ | −0.34±0.03[e] | |
| −4060 | | $\frac{9}{2}^+$ | | 4±2 | 36 | | | | | |
| −1612 | | $\frac{7}{2}^+$ | | 12±2 | 5 | | | | | |

[a]Weaker branches not observed.
[b]Single escape, double-escape yields not included.
[c]Reference 4.
[d]Reference 8.
[e]Reference 6.
[f]Insufficient statistics.

TABLE II. Branching ratios of states above 6.1 MeV compared with the results of Röpke *et al.* (Ref. 5) and SM calculations where applicable. All possible $J_i^\pi$ candidates are listed, derived experimentally as explained in the text. When spin assignments are matched with theory, other possible spins that could not be ruled out from experiment are listed in parentheses.

| $E_i$ (keV) | | | | | BR (%) | | |
|---|---|---|---|---|---|---|---|
| Present | Previous[b] | $E_f$ (keV) | $J_i^\pi$ | $J_f^\pi$ | Present | Previous | SM |
| 6362±4 | 6350 | 0 | $\frac{1}{2}^+, \frac{3}{2}, \frac{5}{2}^+$ | $\frac{5}{2}^+$ | 100[c] | 71 | |
| | | 585 | | $\frac{1}{2}^+$ | | 15 | |
| | | 1965 | | $\frac{5}{2}^+$ | | 8 | |
| | | 975 | | $\frac{3}{2}^+$ | | 6 | |
| 6435±2 | 6425 | 1612 | $\frac{5}{2}^+, \frac{7}{2}, \frac{9}{2}^+$ | $\frac{7}{2}^+$ | 41±8[c] | 19 | |
| | | 3908 | | $\frac{5}{2}^+$ | 14±5[c] | 27 | |
| | | 4060 | | $\frac{9}{2}^+$ | 7±4[c] | 14 | |
| | | 4711 | | $\frac{9}{2}^+$ | 17±7 | 15 | |
| | | 5012 | | $\frac{7}{2}^+$ | 21±7 | 25 | |
| 6842±2 | 6827 | 0 | $\frac{3}{2}^+, \frac{5}{2}, \frac{7}{2}, \frac{9}{2}^+$ | $\frac{5}{2}^+$ | 18±10[c] | 4 | |
| | | 2738 | | | 79±8 | 96 | |
| | | 5012 | | | 3±2[c] | | |
| 6881±2 | 6873 | 1612 | | $\frac{7}{2}^+$ | (100)[c] | 69 | |
| | | 975 | | $\frac{3}{2}^+$ | a | 31 | |
| 6911±3 | 6900 | 0 | $\frac{1}{2}^+, \frac{3}{2}, \frac{5}{2}, \frac{7}{2}^+$ | $\frac{5}{2}^+$ | 100[c] | 77 | |
| | | 2801 | | $\frac{3}{2}^+$ | | 23 | |
| 6958±2 | 6943 | 0 | $\frac{1}{2}^+, \frac{3}{2}, \frac{5}{2}, \frac{7}{2}^+$ | $\frac{5}{2}^+$ | 100[c] | 76 | |
| | | 975 | | $\frac{3}{2}^+$ | | 24 | |
| 7184±2 | 7173 | 1612 | $\frac{3}{2}^+, \frac{5}{2}, \frac{7}{2}, \frac{9}{2}^+$ | $\frac{7}{2}^+$ | 56±16 | 76 | |
| | | 1965 | | $\frac{5}{2}^+$ | 44±16 | 24 | |
| 7225±3 | 7216 | 0 | $\frac{1}{2}^+, \frac{3}{2}, \frac{5}{2}, \frac{7}{2}^+$ | $\frac{5}{2}^+$ | 100[c] | 86 | |
| | | 2801 | | $\frac{3}{2}^+$ | | 14 | |
| 7287±3 | 7270 | 0 | | $\frac{5}{2}^{+c,d}$ | 54±16 | 63 | |
| | | 1965 | | $\frac{5}{2}^{+c}$ | 46±16 | 30 | |
| | | 1612 | | $\frac{7}{2}^+$ | | 7 | |
| 7493±2 | | 4060 | $\frac{11}{2}^+(\frac{9}{2}^+, \frac{11}{2}^-, \frac{13}{2}^+)$ | $\frac{9}{2}^+$ | 68±8 | | 37 |
| | | 5462 | | $\frac{13}{2}^+$ | 28±4 | | 15 |
| | | 5972 | | $\frac{9}{2}^+$ | 4±2 | | 5 |
| | | 1612 | | $\frac{7}{2}^+$ | | | 9 |
| | | 2738 | | $\frac{7}{2}^+$ | | | 3 |
| | | 3405 | | $\frac{9}{2}^+$ | | | 9 |
| | | 5533 | | $\frac{11}{2}^+$ | | | 15 |
| 7501±3 | 7492 | 2738 | $\frac{5}{2}, \frac{7}{2}^+$ | $\frac{7}{2}^+$ | 100[c] | 38 | |
| | | 975 | | $\frac{3}{2}^+$ | | 37 | |
| | | 0 | | $\frac{5}{2}^+$ | | 25 | |
| 7526±3 | 7515 | 2738 | $\frac{5}{2}, \frac{7}{2}, \frac{9}{2}^+$ | $\frac{7}{2}^+$ | 100[c] | 61 | |
| | | 0 | | $\frac{5}{2}^+$ | | 39 | |
| 7550±1 | | 3405 | $\frac{13}{2}^+$ | $\frac{9}{2}^+$ | 23±7 | | 28 |
| | | 5251 | | $\frac{11}{2}^+$ | 50±7 | | 61 |
| | | 5533 | | $\frac{11}{2}^+$ | 18±5 | | 4 |
| | | 5462 | | $\frac{13}{2}^+$ | 9±3 | | 7 |
| 7653±3 | 7639 | 2738 | $\frac{7}{2}, \frac{9}{2}, \frac{11}{2}^+$ | $\frac{7}{2}^+$ | 100[c] | >70 | |
| 7685±3 | | 4060 | $\frac{7}{2}^+, \frac{9}{2}, \frac{11}{2}, \frac{13}{2}^+$ | $\frac{9}{2}^+$ | 100[c] | | |
| 7801±2 | | 1612 | $\frac{7}{2}^+, \frac{9}{2}, \frac{11}{2}^+$ | $\frac{7}{2}^+$ | 97±2[d] | | |
| | | 3405 | | $\frac{9}{2}^+$ | 3±2[c] | | |
| 7866±2 | | 2738 | $\frac{11}{2}^+(\frac{7}{2}^+, \frac{9}{2})$ | $\frac{7}{2}^+$ | 29±13[c] | | 21 |
| | | 3405 | | $\frac{9}{2}^+$ | 33±16 | | 49 |
| | | 4060 | | $\frac{9}{2}^+$ | 21±10[c] | | 4 |
| | | 5533 | | $\frac{11}{2}^+$ | 17±7[c] | | 6 |
| | | 5012 | | $\frac{7}{2}^+$ | | | 9 |

TABLE II. (*Continued*).

| $E_1$ (keV) | | | | | BR (%) | | |
|---|---|---|---|---|---|---|---|
| Present | Previous[b] | $E_f$ (keV) | $J_i^\pi$ | $J_f^\pi$ | Present | Previous | SM |
| | | 5251 | | $\frac{11}{2}^+$ | | | 5 |
| 8 011±2 | | 4711 | $\frac{9}{2}, \frac{11}{2}, \frac{13}{2}^+$ | $\frac{9}{2}^+$ | 100[c] | | |
| 8 074±3 | 8063 | 1612 | $\frac{7}{2}^+, \frac{9}{2}, \frac{11}{2}^+$ | $\frac{7}{2}^+$ | 100[c] | > 70 | |
| 8 264±5 | | 1612 | $\frac{7}{2}^+, \frac{9}{2}, \frac{11}{2}^+$ | $\frac{7}{2}^+$ | 100[c] | | |
| 8 534±2 | | 3405 | $\frac{7}{2}^+, \frac{9}{2}, \frac{11}{2}, \frac{13}{2}^+$ | $\frac{9}{2}^+$ | 76±11[d] | | |
| | | 4711 | | $\frac{9}{2}^+$ | 24±11 | | |
| 8 550±2 | | 1612 | $\frac{7}{2}^+, \frac{9}{2}, \frac{11}{2}^+$ | $\frac{7}{2}^+$ | 31±13[d] | | |
| | | 4060 | | $\frac{9}{2}^+$ | 69±13 | | |
| 8 811±3 | | 4711 | $\frac{7}{2}^+, \frac{9}{2}, \frac{11}{2}, \frac{13}{2}^+$ | $\frac{9}{2}^+$ | 100[c] | | |
| 8 895±1 | | 5793 | $\frac{9}{2}^-, \frac{11}{2}^-(\frac{11}{2}^+)$ | $\frac{11}{2}^-$ | 96±3 | | |
| | | 4060 | | $\frac{9}{2}^+$ | 4±3[c] | | |
| 9 013±2 | | 4711 | $\frac{11}{2}^+(\frac{13}{2}^+)$ | $\frac{9}{2}^+$ | 57±15[c,d] | | 45 |
| | | 5251 | | $\frac{11}{2}^+$ | 43±15[c] | | 16 |
| | | 3405 | | $\frac{9}{2}^+$ | | | 7 |
| | | 4060 | | $\frac{9}{2}^+$ | | | 15 |
| | | 5972 | | $\frac{9}{2}^+$ | | | 10 |
| | | 5533 | | $\frac{11}{2}^+$ | | | 2 |
| | | 5462 | | $\frac{13}{2}^+$ | | | 2 |
| 9 650±3 | | 5462 | $\frac{15}{2}^+(\frac{11}{2}^+, \frac{13}{2}, \frac{17}{2}^+)$ | $\frac{13}{2}^+$ | 100 | | 87 |
| | | 5251 | | $\frac{11}{2}^+$ | | | 7 |
| | | 7550 | | $\frac{13}{2}^+$ | | | 3 |
| 9 685±2 | | 3405 | $\frac{11}{2}^+(\frac{13}{2}^+)$ | $\frac{9}{2}^+$ | 63±7[d] | | NA |
| | | 5533 | | $\frac{11}{2}^+$ | 37±7[d] | | |
| 9 949±2 | | 5251 | $\frac{15}{2}^+$ | $\frac{11}{2}^+$ | 4±2[c] | | 22 |
| | | 5462 | | $\frac{13}{2}^+$ | 45±9[d] | | 22 |
| | | 7550 | | $\frac{13}{2}^+$ | 51±8 | | 43 |
| | | 6041 | | $\frac{11}{2}^+$ | | | 9 |
| | | 8026(SM) | | $\frac{13}{2}^+$ | | | 3 |
| 10 137±4 | | 5533 | $\frac{11}{2}^+, \frac{13}{2}, \frac{15}{2}^+$ | $\frac{11}{2}^+$ | 100 | | |
| 10 653±2 | | 5533 | $\frac{15}{2}^+$ ( $\frac{13}{2}^-$) | $\frac{11}{2}^+$ | 94±3[d] | | 41 |
| | | 7550 | | $\frac{13}{2}^+$ | 6±3[c] | | 23 |
| | | 6041 | | $\frac{11}{2}^+$ | | | 9 |
| | | 5462 | | $\frac{13}{2}^+$ | | | 14 |
| | | 8026(SM) | | $\frac{13}{2}^+$ | | | 11 |
| 11 004±3 | | 5462 | $\frac{17}{2}^+(\frac{15}{2}^+)$ | $\frac{13}{2}^+$ | 100 | | 88 |
| | | 9949 | | $\frac{15}{2}^+$ | | | 11 |
| 11 361±3 | | 5793 | $\frac{13}{2}^-, \frac{15}{2}^-$ | $\frac{11}{2}^-$ | 100 | | |
| 11 410±3 | | 5462 | $\frac{15}{2}^+, \frac{17}{2}^+$ | $\frac{13}{2}^+$ | 91±3[d] | | |
| | | 7550 | | $\frac{13}{2}^+$ | 9±3[c] | | |
| 11 460±3 | | 5251 | $\frac{11}{2}^+, \frac{13}{2}, \frac{15}{2}^+$ | $\frac{11}{2}^+$ | < 39 | | |
| | | 5462 | | $\frac{13}{2}^+$ | > 61 | | |
| 11 486±6 | | 5462 | $\frac{11}{2} - \frac{15}{2}$ | $\frac{13}{2}^+$ | < 38 | | |
| | | 8011 | | $\frac{9}{2}, \frac{11}{2}, \frac{13}{2}^+$ | > 62 | | |
| 13 143±4 | | 5793 | $\frac{11}{2}^-, \frac{13}{2}, \frac{15}{2}^-$ | $\frac{11}{2}^-$ | 100[c] | | |
| 13 332±10 | | 5462 | $\frac{13}{2}^+, \frac{15}{2}, \frac{17}{2}^+$ | $\frac{13}{2}^+$ | 100[e] | | |

[a]Same energy as SE, 6958 keV.
[b]Reference 5; all errors are ±3 keV; relative branching ratio errors are 10– 30% (weaker transitions).
[c]158° detector only.
[d]No SE or DE yields included.
[e]120° detector only.

TABLE III. Angular correlation results for states in $^{25}$Mg measured in the present work, compared with shell model (SM) predictions for positive parity. Also listed are theoretical lifetimes with no inclusion of particle decay. The Legendre polynomial coefficients were taken at the minimum in $\chi^2$ vs $\delta$. Uncertainties are not listed for these coefficients because only three angles were measured.

| $E_i - E_f$ (keV) | $J_i^\pi$ | $J_f^\pi$ | $A_2/A_0$ | $A_4/A_0$ | $\delta$ expt | $\delta$ SM | $\tau^{SM}$ (fsec) |
|---|---|---|---|---|---|---|---|
| 7 550-5251 | $\frac{13}{2}^+$ | $\frac{11}{2}^+$ | −0.69 | 0.023 | 0.23±0.04 | 0.14 | 3.7 |
| -3405 | $\frac{13}{2}^+$ | $\frac{9}{2}^+$ | | | | 0.0 | |
| -5462 | $\frac{13}{2}^+$ | $\frac{13}{2}^+$ | | | | -0.15 | |
| -5533 | $\frac{13}{2}^+$ | $\frac{11}{2}^+$ | | | | 0.15 | |
| 8 895-5793 | $\frac{9}{2}^-$ | $\frac{11}{2}^-$ | 0.55 | 0.075 | $0.93^{+0.44}_{-0.33}$ | | |
| | $\frac{11}{2}$ | $\frac{11}{2}^-$ | 0.53 | −0.038 | $-0.31^{+0.26}_{-0.29}$ | | |
| | $\frac{13}{2}^+$ | $\frac{11}{2}^-$ | 0.69 | 0.15 | $-0.70^{+0.15}_{-0.27}$ | | |
| 9 949-7550 | $\frac{15}{2}^+$ | $\frac{13}{2}^+$ | −0.51 | 0.0 | 0.16±0.04 | 0.09 | 4.1 |
| -5462 | | $\frac{13}{2}^+$ | −0.18 | 0.0 | −0.05±0.05 | 0.42 | |
| | | | −0.33 | 0.44 | $7.1^{+12}_{-2.6}$ | | |
| 11 486-8011 | $J+1$ | $J$ | −0.63 | 0.016 | $0.19^{+0.32}_{-0.19}$ | | |
| | | | −0.75 | 0.39 | 2.48±0.68 | | |
| | $J-1$ | $J$ | −0.61 | 0.015 | $-0.29^{+0.24}_{-0.44}$ | | |
| | | | −0.66 | 0.18 | $-3.7^{+1.8}_{-10.6}$ | | |

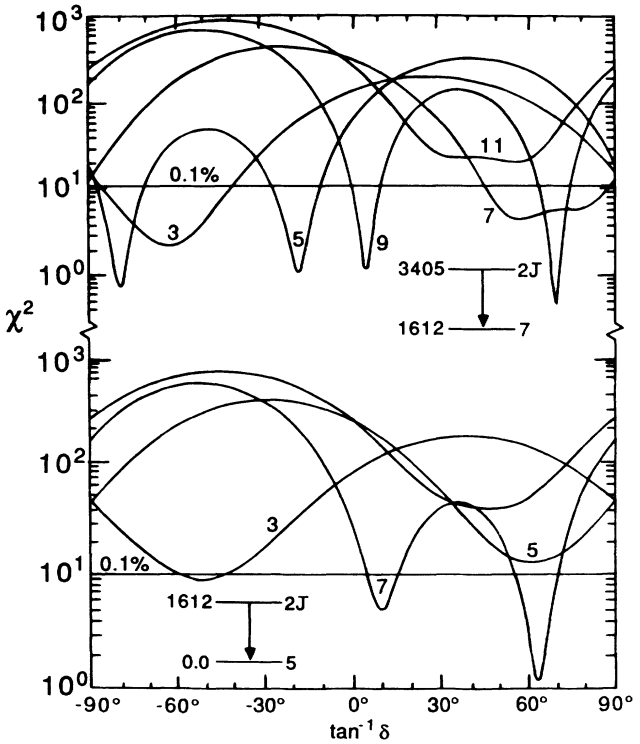


FIG. 6. Graphs of the reduced $\chi^2$ vs $\tan^{-1}\delta$ for the $\frac{9}{21}^+ \rightarrow \frac{7}{21}^+$ (upper) and $\frac{7}{21}^+ \rightarrow \frac{5}{21}^+$ transitions in $^{25}$Mg. Energies for initial and final states are given in keV, and $\chi^2$ is plotted for different values of $2J_i$ while fixing $J_f$ to the known value. The 0.1% confidence level is drawn as a solid horizontal line for $\chi^2 = 10.8$. Although more than one $J_i$ is acceptable at the 0.1% limit, the minima in $\chi^2$ nearest $\delta = 0$ for the correct spins reproduce earlier work.

sible mixing ratio value of $\delta = 0.23 \pm 0.04$, which is quite consistent with the mixing ratios known for six other $M1+E2$ transitions. It is less likely that the 7550-keV level has spin $\frac{9}{2}^+$ because many possible decay branches would be available to such a state, while the actual branches decay to many of the lowest levels available to the decay of a $\frac{13}{2}^+$ state. As discussed below, an assignment of $\frac{13}{2}^+$ to the 7550-keV state is almost certain due to the decay branches from the 9949 and 11410-keV states as well as to correspondence with SM predictions. In turn, this establishes the assignment of $\frac{11}{2}^+$ to the 5251-keV level.

The angular correlation fits for the 8895→5793-keV transition are shown in Fig. 8, assuming a spin of $\frac{11}{2}$ for the 5793-keV level. The graphs would be rather similar for the other spin possibility of $\frac{7}{2}$ if all spin labels were reduced accordingly. This decay branch for either possible final spin and another observed decay to the second $\frac{9}{2}^+$ state limit the possible spins of the 8895-keV level to $\frac{5}{2}^+$, $\frac{7}{2}^\pm$, $\frac{9}{2}^\pm$, $\frac{11}{2}^\pm$, and $\frac{13}{2}^+$. The fact that these $\gamma$ decays exist in competition with neutron decay further limits the possible spin-parity values to $\frac{9}{2}^-$ or $\frac{11}{2}^\pm$.

Angular correlation results for two decays of the 9949-keV level are shown in Fig. 9. The existence of $\gamma$ decay in competition with neutron decay clearly rules out spins below $\frac{11}{2}$. The spin possibility of $\frac{9}{2}$ is also ruled out by the large mixing ratio $|\delta| > 0.19$ for the decay to the 5462-keV $\frac{13}{2}^+$ state (Fig. 9), which would imply an unrealistically large $M3$ component. Possible spin parities of $\frac{11}{2}^+$ or $\frac{13}{2}^+$ for the 9949- keV level are also incompatible with the open $l=4$ neutron channel which would have a width of at least 18 eV if the spectroscopic factor

were greater than 0.01. A comparable $\gamma$ width would imply an $M1$ strength in excess of 30 W.u. for the 50% branch to the 7550-keV level. The smallest $E2$ admixture in this decay is given by the curve labeled 15 in the upper part of Fig. 9, which is basically the $J \rightarrow J-1$ correlation. This mixing ratio of $\delta = 0.16 \pm 0.04$ is in good agreement with other $M1+E2$ transitions, but would imply an $E2$ strength greater than 450 W.u. under the above assumptions of $\frac{11}{2}^+$ or $\frac{13}{2}^+$ for the 9949-keV level. This rather strongly establishes a spin parity of $\frac{15}{2}^+$ for the 9949-keV level. It also establishes the assignment of $\frac{13}{2}^+$ for the 7550-keV state.

TABLE IV. Summary of spin assignments in $^{25}$Mg. Where possible assignments to rotational bands (with Nilsson quantum numbers $[Nn_z\Lambda]\Omega$) or shell-model configurations are given. The subscripts in the spin column index states of the same spin and parity.

| $J^\pi_\#$ | $E_x$ (MeV) | Rotational band assignment |
|---|---|---|
| $\frac{5}{2}^+_1$ | 0.0 | $[202]\frac{5}{2}$ |
| $\frac{1}{2}^+_1$ | 0.585 | $[211]\frac{1}{2}$ |
| $\frac{3}{2}^+_1$ | 0.975 | $[211]\frac{1}{2}$ |
| $\frac{7}{2}^+_1$ | 1.612 | $[202]\frac{5}{2}$ |
| $\frac{5}{2}^+_2$ | 1.965 | $[211]\frac{1}{2}$ |
| $\frac{1}{2}^+_2$ | 2.564 | $[200]\frac{1}{2}+(K-2)_\gamma$ on $[202]\frac{5}{2}$ |
| $\frac{7}{2}^+_2$ | 2.738 | $[211]\frac{1}{2}$ |
| $\frac{3}{2}^+_2$ | 2.801 | $[200]\frac{1}{2}+(K-2)_\gamma$ |
| $\frac{9}{2}^+_1$ | 3.405 | $[202]\frac{5}{2}$ |
| $\frac{3}{2}^-_1$ | 3.414 | $[330]\frac{1}{2}$ |
| $\frac{5}{2}^+_3$ | 3.908 | $[200]\frac{1}{2}+(K-2)_\gamma$ |
| $\frac{7}{2}^-_1$ | 3.971 | $[330]\frac{1}{2}$ |
| $\frac{9}{2}^+_2$ | 4.060 | $(K+2)_\gamma$ on $[202]\frac{5}{2}$ or $[\pi(d_{5/2})^{-2}\nu(d_{5/2})^{-2}]^{-1}$ (triaxial) |
| $\frac{1}{2}^-_1$ | 4.277 | $[300]\frac{1}{2}$ |
| $\frac{3}{2}^+_3$ | 4.359 | $[211]\frac{3}{2}+(K-2)_\gamma$ on $[211]\frac{1}{2}$ |
| $\frac{9}{2}^+_3$ | 4.711 | $[211]\frac{1}{2}$ |
| $(\frac{5}{2}^+_4)$ | 4.722 | $[211]\frac{3}{2}+(K-2)_\gamma$ |
| $\frac{7}{2}^+_3$ | 5.012 | $[200]\frac{1}{2}+(K-2)_\gamma$ |
| $\frac{1}{2}^-_2$ | 5.116 | |
| $\frac{11}{2}^+_1$ | 5.251 | $[211]\frac{1}{2}$ or $(K+2)_\gamma$ on $[202]\frac{5}{2}$ |
| $\frac{13}{2}^+_1$ | 5.462 | $[\pi(d_{5/2})_4^{-2}\nu(d_{5/2}^{-1}]_{13/2}$ |
| $\frac{1}{2}^+_3$ | 5.475 | |
| $\frac{5}{2}^-_1$ | 5.521 | $[330]\frac{1}{2}$ |
| $\frac{11}{2}^+_2$ | 5.533 | $[202]\frac{5}{2}$ |
| $(\frac{3}{5})^+$ | 5.747 | |
| $\frac{11}{2}^-_1$ | 5.793 | $[330]\frac{1}{2}$ |
| $\frac{5}{2}^+$ | 5.859 | |
| $\frac{9}{2}^+_4$ | 5.972 | $[200]\frac{1}{2}+(K-2)_\gamma$ |
| $\frac{7}{2}^+_4$ | 5.978 | $[211]\frac{3}{2}+(K-2)_\gamma$ |
| $(\frac{11}{2}^+_3)$ | 6.041 | $(K-2)_\gamma$ on $[202]\frac{5}{2}$ |
| $(\frac{11}{2}^+_4)$ | 7.493 | |
| $\frac{13}{2}^+_2$ | 7.550 | $[202]\frac{5}{2}$ |
| $(\frac{11}{2}^+_5)$ | 7.866 | |
| $(\frac{9}{2}^-_1)$ | 8.895 | $[330]\frac{1}{2}$; $\pi[211]\frac{3}{2}[330]\frac{1}{2}$ , $\nu(211]\frac{1}{2}$ |
| $(\frac{11}{2}^+_7)$ | 9.013 | |
| $(\frac{15}{2}^+_1)$ | 9.650 | |
| $(\frac{11}{2}^+_9)$ | 9.685 | |
| $\frac{15}{2}^+_2$ | 9.949 | |
| $(\frac{15}{2}^+_3)$ | 10.653 | $[202]\frac{5}{2}$ |
| $(\frac{17}{2}^+_1)$ | 11.004 | $[\pi(d_{5/2})_4^{-2}\nu(d_{5/2})_4^{-2}(\frac{1}{2})^+_{1/2}]\frac{17}{2}$ |

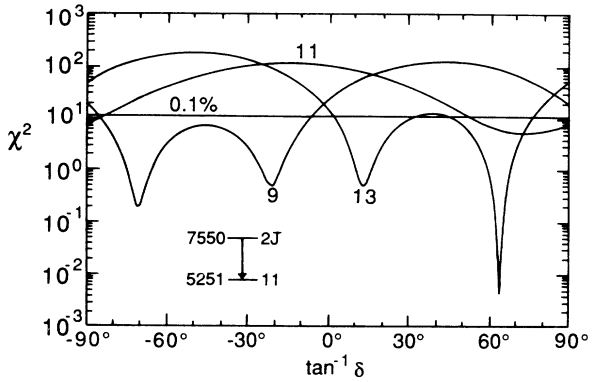


FIG. 7. A graph of $\chi^2$ vs $\tan^{-1}\delta$ for the 7550-keV$\rightarrow \frac{11}{2}^+_1$ transition in $^{25}$Mg. Notation is the same as in Fig. 6.

For the 10653-keV state, $\gamma$ decays to the $\frac{11}{2}^+_2$ and $\frac{13}{2}^+_2$ states limit its possible spin-parity values to $\frac{9}{2}^+$, $\frac{11}{2}^\pm$, $\frac{13}{2}^\pm$, and $\frac{15}{2}^+$. The competition from neutron decay rules out the $\frac{9}{2}^+$, $\frac{11}{2}^\pm$, and $\frac{13}{2}^+$ possibilities. Since the state decays only to positive parity levels, $\frac{13}{2}^-$ is less likely. Thus the 10653-keV state most likely has a spin parity of $\frac{15}{2}^+$.

The 11004-keV state was observed to decay only to the lowest $\frac{13}{2}^+$ state. The competition with neutron decay rules out possible spins for this state below $\frac{15}{2}$. The possibility of $\frac{15}{2}^-$ is unlikely since it would imply an $E1$ decay strength three times greater than the upper limit of 0.03 W.u. Therefore, the 11004-keV state is a good candidate to be the yrast $\frac{17}{2}^+$ state, although it could also have a spin parity of $\frac{15}{2}^+$.

An observed state at 11 361 keV decays solely to the 5793-keV level, which has a spin parity of $\frac{11}{2}^-$ or $\frac{7}{2}^-$. This decay rules out the $\frac{7}{2}^-$ possibility for the 5793-keV state because the highest possible spin of the 11 361-keV state ($\frac{11}{2}^-$) would still lead to an $E2$ strength far in excess

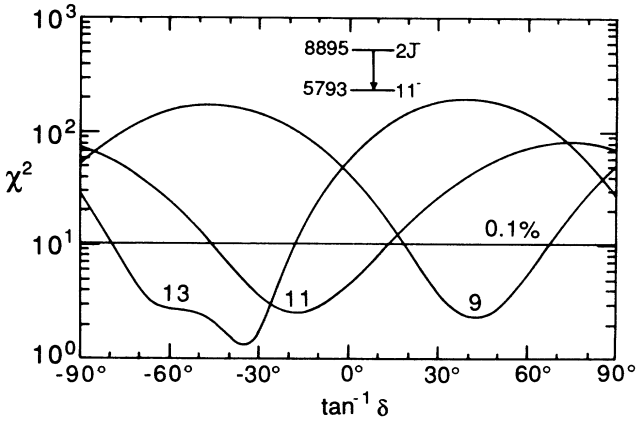


FIG. 8. A graph of $\chi^2$ vs $\tan^{-1}\delta$ for the 8895-keV$\rightarrow \frac{11}{2}^-_1$ transition. Notation is the same as in Fig. 6.

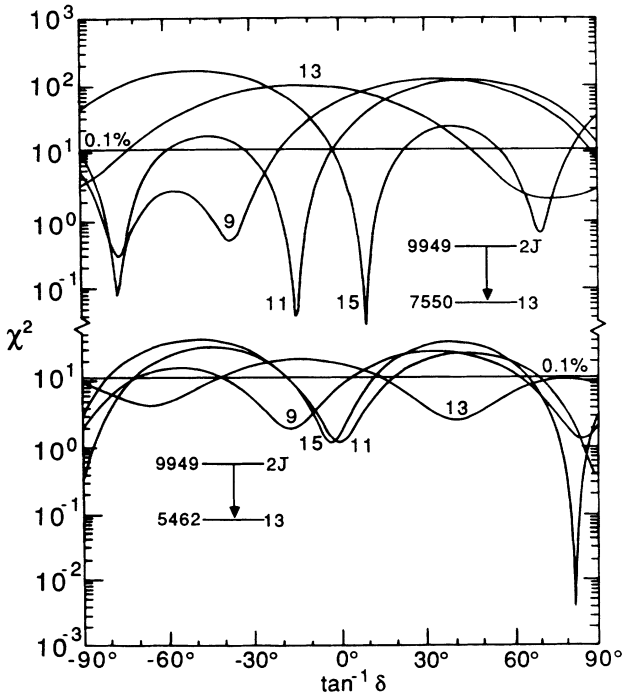


FIG. 9. Graphs of $\chi^2$ vs $\tan^{-1}\delta$ for the 9949→7550-keV transition (upper) and the 9949-keV→$\frac{13}{2}_1^+$ transition. Notation is the same as in Fig. 6.

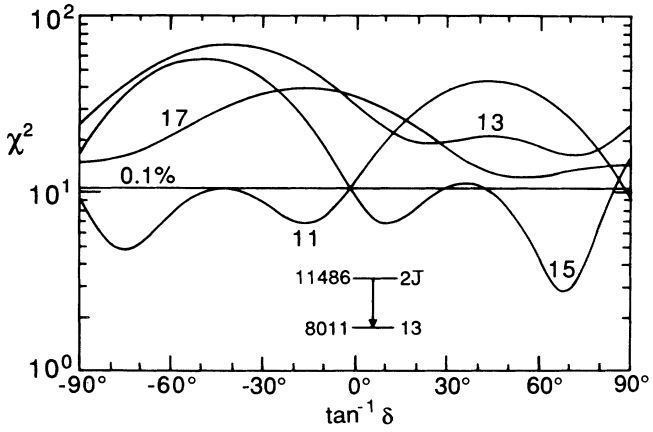


FIG. 10. A graph of $\chi^2$ vs $\tan^{-1}\delta$ for the 11 486→8011-keV transition. The spin of the 8011-keV state was set at $\frac{13}{2}$ for this plot, but $\frac{9}{2}$ or $\frac{11}{2}$ are also possible. Only $J+1\rightarrow J$ or $J-1\rightarrow J$ transitions are acceptable at the 0.1% limit.

of 100 w.u. when the neutron-decay competition is considered. Thus the decay to an $\frac{11}{2}^-$ state limits the spin parity of the 11 361-keV level to $\frac{13}{2}^-$ or $\frac{15}{2}^-$.

The 11 410-keV state decays to the yrast $\frac{13}{2}^+$ state and the tentative second $\frac{13}{2}^+$ state at 7550 keV. The competition with neutron decay of the 5949-keV $\gamma$ transition to the $\frac{13}{2}_1^+$ level rules out all spins below $\frac{15}{2}$ as well as the $\frac{15}{2}^-$ possibility. Therefore the 11 410-keV state has a spin parity of $\frac{15}{2}^+$ or $\frac{17}{2}^+$. This assignment rules out $\frac{9}{2}^+$ for the 7550-keV state, since it would imply an $M3$ decay, and in turn rules out $\frac{7}{2}^+$ for the 5251-keV state.

Figure 10 displays $\chi^2$ versus $\delta$ for the 11 486→8011-keV transitions. $J_f$ was set to $\frac{13}{2}^+$ for the calculation but it could also be $\frac{7}{2}$ through $\frac{11}{2}$ if all the spin labels were appropriately reduced. The results in Fig. 10 rule out the combinations $J\rightarrow J$ and $J+2\rightarrow J$ for this $\gamma$ ray and, when combined with neutron-decay estimates, assign $J=\frac{11}{2}$, $\frac{13}{2}$, or $\frac{15}{2}$ for the 11 486-keV state.

Spin assignments to the 7493, 7866, 9013, 9650, and 9685-keV states are discussed in Sec. V C in conjunction with theoretical predictions.

## IV. THEORETICAL METHODS

### A. The *s-d* shell model

The shell-model predictions with which the present experimental results are compared are generated in the full $0d_{5/2}$-$1s_{1/2}$-$0d_{3/2}$ orbital space with the unified *s-d* (USD) model Hamiltonian.[22] The USD Hamiltonian was determined by iteratively varying the two-body matrix elements and single-particle energies which define it while requiring an rms minimum between shell-model eigenvalues and the experimentally measured energies of some 440 corresponding nuclear levels in $A=17-39$ nuclei. Most of these levels are well-identified low-lying states in $A=18-24$ and $A=32-38$ nuclei. The larger matrix dimensions associated with states near the middle of the *s-d* shell, with the resulting requirements on computer time, precluded treatment of most spins in the $A=25-31$ region. Those data which were included were, for the most part, the energies of $0^+$ and $\frac{1}{2}^+$ states, since these spins correspond to the smallest dimensionalities. A key aspect of obtaining a single set of Hamiltonian parameters which describe the entire range of *s-d* shell masses was found to be a mass-dependent scale factor for the two-body matrix elements. The USD mass dependence was set at $A^{-0.3}$.

The fundamental assumptions of the USD calculations are that the preponderance of low-lying states in $A=18-38$ nuclei are manifestations of *s-d* shell degrees of freedom, that the complete set of *s-d* shell basis vectors provides a reasonably uniform model approximation for these states, and that a single formulation of the model Hamiltonian, in the context of the USD approach, can subsume all of the dynamical structures inherent in this vector space. It is to be noted that the USD approach makes no assumptions about the nature of the model Hamiltonian other than that it is $0+1+2$ body in nature, conserves isospin, and has the mass dependence noted.

The rms derivation between the 440 USD eigenvalues and the presumed corresponding experimental states which were used in the iterative fits is 150 keV. This quality of agreement is good enough, in the context of the various approximations inherent in the approach, to suggest that the basic assumptions of the model may be valid. The next stage of validation of the approach was calculation of the energies of the remaining unexamined states in the $A=25-31$ region. The rms deviation between predictions and experiment for these additional

several hundred levels was smaller than 150 keV, a result understandable as indicating that the model assumptions are better in the center of the shell than near its boundaries.

The remaining areas of validity testing of the model results are twofold; namely, testing energy predictions against new data on states of extreme configurations, either high $J$ or high $T$ (large neutron-proton asymmetries) and testing wave-function predictions by comparisons with various moment and transition-rate data. In the latter mode, various systematic studies[23,24] have confirmed that, with simple renormalizations of the standard operators, electromagnetic and weak data are well predicted with the USD wave functions. The operator renormalizations can be understood as very economical compensations for the effects of the vast array of excluded shell-model orbits, as well as of mesonic-exchange currents, nucleon excitations, and so on.

In the present work, the USD predictions for the energies of higher-excitation, higher-spin states in $A=25$, $T=\frac{1}{2}$ are compared with new experimental results, along with comparisons between predicted and observed electromagnetic decays of these and lower-lying states. In essence, the question is whether the high-spin structures between 5 and 10 MeV in $^{25}$Mg are consistent, in energy and configuration mixing, with the preponderance of nuclear structure phenomena of $A=18-38$ data in the 0–5 MeV excitation range—phenomena which the USD Hamiltonian in the full $s$-$d$ shell space can be considered to accurately model. Of particular interest in $A=25$ is the question of whether the anomalous structure of $8^+$ states in $^{24}$Mg has an analogy in $^{25}$Mg–$^{25}$Al. In $^{24}$Mg the USD Hamiltonian and its precursors[25,26] predict[27] an yrast $8^+$ state which is more "spherical" than the $8^+$ member of either the $K=0$ or $K=2$ rotational bands and which, in the absence of lower-lying states of lower spin to which it is coupled, could be considered a $K=8$ bandhead. Experiment[28] subsequently confirmed the existence of an yrast $8^+$ state which apparently corresponded to this prediction. It is important to know whether this phenomenon is more or less a random coincidence or whether it reflects some deeper structural relationship.

### B. The cranked Nilsson-Strutinsky model

In the cranked Nilsson-Strutinsky model[29] (CNSM) all relevant $N$ shells are considered, and the coupling between them is accounted for. The nucleus is allowed to deform to find the most favorable shape, but apart from the rotating deformed field, no additional residual interactions are included. Thus, no very detailed description of the observed spectrum can be expected. This is especially true at low spins where pairing correlations appear important and where the cranking approximation with the spin vector pointing along one principal axis (in the intrinsic system) is questionable. On the other hand, we can expect to describe the main features of the spectrum up to the highest spins, including states with particles or holes outside the $N=2$ shell. Additionally, the model gives a transparent description of the different rotational bands, band terminations, and particle-hole states.

In the present formalism,[30] different configurations are fixed by the number of particles in different $N$ shells in the rotating frame ($N_{\rm rot}$) and the number of particles of different signature ($\alpha$) within each of these shells. For an odd nucleus such as $^{25}$Mg, $\alpha_{\rm tot}=\sum_i \alpha_i \bmod 2=+\frac{1}{2}$ gives $J=\frac{1}{2},\frac{5}{2},\frac{9}{2},\ldots$, while $\alpha_{\rm tot}=-\frac{1}{2}$ gives $J=\frac{3}{2},\frac{7}{2},\ldots$. Since $\sum_i (N_{\rm rot})_i$ determines the total parity $\pi_{\rm tot}$, configurations can be labeled by the symbols $(\pi_{\rm tot},\alpha_{\rm tot})$ which breaks up the yrast line into four lines. The energies of each configuration are calculated as a function of spin by a minimization in the deformation degrees of freedom, $\epsilon_2$, $\epsilon_4$, and $\gamma$, for each spin and each configuration.

The formalism is similar to that used[13] for a large number of other $s$-$d$ shell nuclei with, however, some minor differences. First, the moment of inertia has been renormalized to the rigid-body value using the Strutinsky procedure, whereas in Ref. 13, the spin dependence of the energy was taken directly from the sums of the single-particle energies. With the present method, it seems that the energy will increase somewhat faster with spin (smaller moment of inertia), while for fixed spin the ordering and spacing between the states will be essentially unchanged.

The second major difference is due to the fact that the present results are calculated in a rotating harmonic oscillator basis where the couplings between $N_{\rm rot}$ shells, essentially due to $\epsilon_4$ deformations, are neglected. At the small ($\epsilon \leq 0.45$) deformations we consider here and with the average deformation dependence normalized to the liquid drop formula, such an approximation is clearly justified. The advantage of this approximation is that, with $N_{\rm rot}$ as a conserved quantum number, it becomes possible to distinguish in a much more precise way between different configurations. Thus, for all spins, pure $s$-$d$ shell configurations are easily distinguished from those with one particle in the $f$-$p$ shell which in turn are distinguished from configurations with two particles in the $f$-$p$ shell, etc. Similarly, configurations with holes in the $p$ shell can be followed for all spins. The signature quantum number of individual orbitals then gives additional possibilities to distinguish between configurations.

The liquid drop parameters are the same as in Refs. 13, 29, and 30. The $ls$ and $l^2$ coupling strengths are chosen as $\kappa=0.08$ and $\mu=0.0$, respectively, for protons as well as neutrons.[13] As we will find below when comparing to experiment, this choice is not optimal. However, we find it questionable to try to optimize these parameters for each individual nucleus but rather want to consider the present calculations as a help in finding better parameters which can be used for all or at least a large number of $s$-$d$ shell nuclei.

Pairing has been neglected in the present calculations, and the total energy for some fixed deformation $\epsilon$, $\epsilon_4$, and $\gamma$, and spin $J$ becomes

$$E_{\rm tot}(J)=\Sigma e_i^{\omega}+\omega\Sigma\langle j_x\rangle_i-\langle E_{\rm sp}(J)\rangle + \Delta E_{\rm surf}+\Delta E_{\rm Coul}+\hbar^2 J^2/2\mathcal{J}_{\rm rig}\,, \tag{5}$$

where all quantities are evaluated at the same spin $J$. In

Eq. (5), $e_i^{\omega}$ are single-particle Routhians. Surface and Coulomb energies are taken relative to their values at spherical shape,

$$\Delta E_{\text{surf}} = E_{\text{surf}}(\epsilon_2,\epsilon_4,\gamma) - E_{\text{surf}}(0,0,0) ,$$

$$\Delta E_{\text{Coul}} = E_{\text{Coul}}(\epsilon_2,\epsilon_4,\gamma) - E_{\text{Coul}}(0,0,0) ,$$

while $\mathcal{J}_{\text{rig}}$ is the rigid body moment of inertia calculated at the appropriate deformation. For each spin, the energy (5) is calculated in a mesh in $\epsilon_2$, $\epsilon_4$, and $\gamma$ and the minimum then defines the energy of the configuration in question.

## V. COMPARISON OF EXPERIMENT AND THEORY

In this section we compare both models with experiment, and therefore intermix collective model concepts (rotational bands and $K$ quantum numbers) with SM results.

### A. Levels below 6.1 MeV with $J \leq \frac{11}{2}$

Previously known energy levels and spins for $E_x < 6.1$ MeV are shown in Fig. 11 and are compared with the positive parity states of the SM calculations on the left and the negative parity states of the CNSM on the right. Of the 25 positive parity states in Fig. 11, the SM agrees remarkably well with all but the 5971-keV $\frac{9}{2}^+$ state; this state is predicted in the SM at 6306 keV. Disagreement exists in the literature on the $J^{\pi}$ of the 4722-keV state[8,9] where both $\frac{5}{2}^+$ and $(\frac{1}{2},\frac{3}{2}^-)$ have been proposed, and on the parity of the $\frac{5}{2}$ states at 5521 and 5859 keV.[6,10,31] The $\frac{5}{2}^+$ SM states corresponding to the observed 4722- and 5859-keV states reinforce that assignment of spin and parity for these levels, making the 5521-keV experimental state the $\frac{5}{2}^-$ member of the $[330]\frac{1}{2}$ Nilsson orbital's rotational band. Also, the $\frac{5}{2}^+$, $\frac{11}{2}^+$, and $\frac{11}{2}^+$ SM states corresponding to the experimental states at 5747, 5251, and 6041 keV, respectively, reinforce these spin assignments, adding more support to rejection of the $\frac{7}{2}^+$ assignment for the latter two states. The $\frac{3}{2}^+$, 5589-keV and $\frac{7}{2}^+$, 6151-keV SM states do not correspond to states experimentally observed below 6.2 MeV.

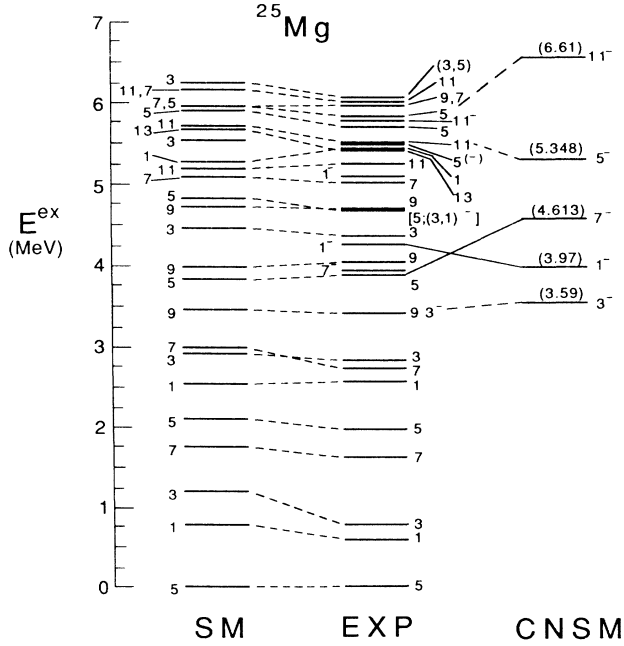


FIG. 11. Comparison of the shell model (SM) and the cranked Nilsson-Strutinsky model (CNSM) with experiment for states below 6.1 MeV in $^{25}$Mg. The SM reproduces all positive-parity states except the 5971 keV, $\frac{9}{2}^+$ state, to within 120±72 keV. Only negative-parity CNSM states have been included. They show a fair correspondence with the lowest $f_{7/2}$ rotational band.

The CNSM complements the SM in providing information on the negative parity states. The calculated members of the $\frac{1}{2}^-$, $\frac{3}{2}^-$, $\frac{5}{2}^-$, $\frac{7}{2}^-$, and $\frac{11}{2}^-$ members of the $[330]\frac{1}{2}$ band are compared with experiment in Fig. 11, where we obtain an average deviation of 423±280 keV. This is quite good considering the fact that for such a high-$j$ band, the cranking concept is very questionable at low spins. Additionally, no attempt is made to optimize energy fits in the CNSM calculations (see also discussion in Sec. V C 5).

For the 24 states in this excitation region observed in the SM calculations, the average deviation of experiment and theory is 120±72 keV. Theoretical branching and mixing ratios are listed in Table I for several states. Overall agreement is fair, with the largest branches generally predicted correctly, with the proper sign and magnitude for δ. The precision of the SM in reproducing the lower-energy experimental states suggests its usefulness in comparing with higher-spin, higher-energy states.

The experimentally derived intrinsic quadrupole moment $Q_0$ for $^{25}$Mg is $+56.3\pm0.8$ fm$^2$.[32] Using the relation

$$Q_0(\text{prolate}) = \tfrac{4}{5} Z A^{2/3} r_0^2 \epsilon_2 (1+\epsilon_2/2)$$

with $r_0 = 1.2$ fm, we obtain $\epsilon_2 = 0.40$ as an estimate of the ground-state quadrupole distortion in $^{25}$Mg. The SM predicts $Q_0 = 52.4$ fm$^2$, corresponding to $\epsilon_2 = 0.37$.

Figure 12 displays Nilsson orbitals for the $1p$ and $1s$-$2d$ shells, including $\epsilon_4$ deformations. At a deformation of $\epsilon_2 = 0.40$, the 13th neutron of $^{25}$Mg occupies the $[211]\frac{1}{2}$ orbital instead of the adjacent $[202]\frac{5}{2}$ orbital as expected for the proper ground-state spin. This discrepancy, and the fact that the CNSM is not designed to accurately reproduce level energies especially for low-spin states, represent the major reasons for excluding the CNSM predictions of level energies in Fig. 11.

Figures 13 and 14 display potential-energy surfaces calculated with the CNSM for selected spins and $(\pi,\alpha)$ combinations. In each diagram, the minimum is represented by a dot, and the calculated excitation energy and deformation at the minimum are given above each surface. The contour line spacing is 1 MeV, and some contour lines are labeled by the energy above the static liquid-drop energy for spherical shape.

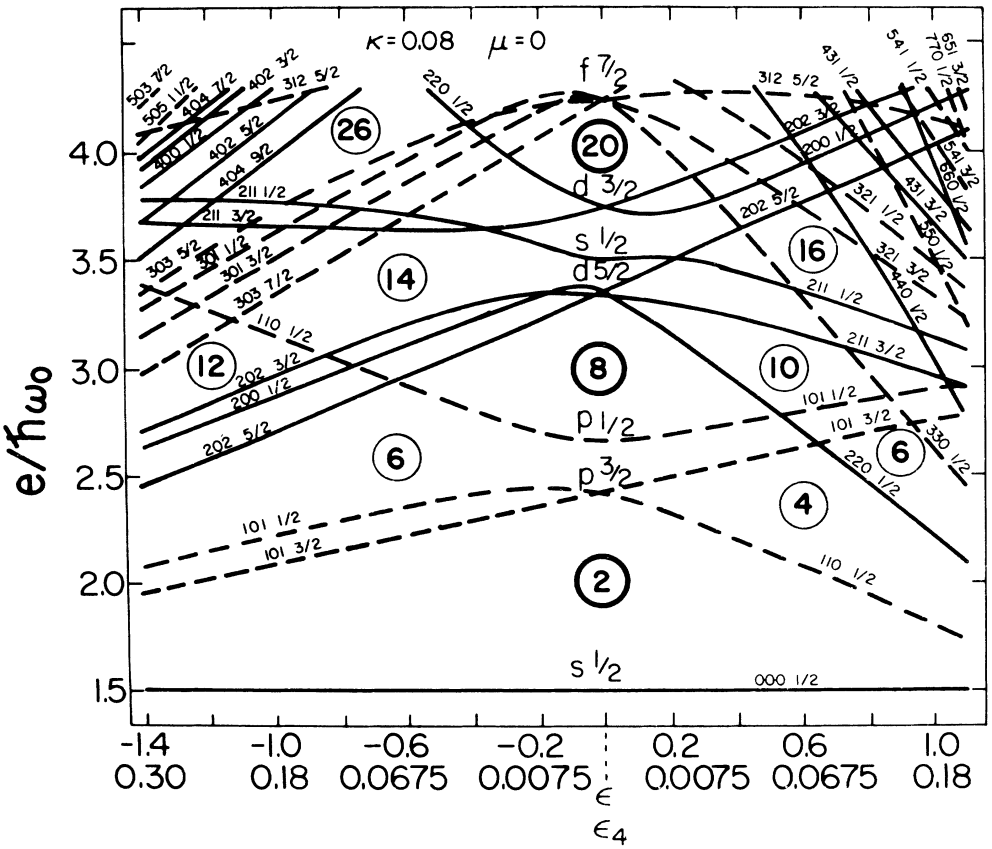


FIG. 12. Static Nilsson orbitals for 1$p$ and 1$s$-2$d$ shells, for prolate ($\epsilon>0$) and oblate deformations. Hexadecapole ($\epsilon_4$) deformations are also included. Numbers in circles are the total particles in a configuration and identify shell closures for a particular deformation. The parameters $\kappa=0.08$ and $\mu=0.0$ are used for both protons and neutrons. Orbitals are labeled by the asymptotic quantum numbers $|Nn_z\Lambda\Omega\rangle$. Couplings between orbitals with $\Delta N=2$ have been included but in order to make the figure easier to read such orbitals have been allowed to cross, e.g., the crossing between $|330\ \frac{1}{2}\rangle$ and $|101\ \frac{1}{2}\rangle$.

For prolate band heads at $\omega=0$ and $\gamma=0°$, $J=J_x=0$ in the cranking formalism so that rotation must be introduced to generate spin. This is not the case for the prolate shape at $\gamma=-120°$ where the spin is measured along the symmetry axis and cranking has no physical significance. Instead, the total spin equals $\Omega$ of the odd particle or the sum of the $\Omega$:$S$ for multiparticle-multihole configurations ($\Omega=m$ being the single-particle spin projection on the symmetry axis). For example, in the $\frac{1}{2}^+$ energy surface of Fig. 13(a), the $\gamma=-120°$ minimum should come somewhat below the $\gamma=0°$ minimum, but in practice this difference is negligible, and the two minima can be considered equivalent.

Figure 13(b) contains $\frac{5}{2}^+$ configurations. A secondary minimum can be seen at $(\epsilon_2,\gamma)=(0.32,-98°)$, 100 keV higher in energy than the ground-state $\frac{5}{2}^+$ band member. The saddle point in two dimensions along the $\gamma=-120°$ axis represents a third energy minimum with a unique configuration and $\epsilon\approx0.2$. This aligned state corresponds to the experimental ground state, predicted to lie at 2.2 MeV in excitation. The disagreement with experiment comes from the $d_{5/2}$-$s_{1/2}$ orbital spacing. Since both the $[202]\frac{5}{2}$ and $[211]\frac{1}{2}$ Nilsson orbitals are $(\pi,\alpha)=(+,+\frac{1}{2})$ configurations in the CNSM, a rotational band built on the $\frac{5}{2}^+$ state could not be generated by the calculations in any straightforward way. The wave function making up the minimum at $\gamma\approx-100°$ in Fig. 13(b) is similer to that of the aligned $\frac{5}{2}^+$ states just mentioned. This means that the spin is mainly built by one aligned neutron. It reflects a tendency towards triaxial shape also seen in the ground state of $^{24}$Mg.[13]

The $\frac{11}{2}^+$ potential energy surface ($\alpha=-\frac{1}{2}$) is displayed in Fig. 14(a). The ground-state band member remains yrast, with $\epsilon_2$ similar to its value in the $\frac{1}{2}^+$ band head, and slightly triaxial with $\gamma\approx6°$. The measured branching ratios suggest that the observed 5533-keV, $\frac{11}{2}^+$ state should be assigned as a member of the $[202]\frac{5}{2}$ ground-state band. A local minimum also exists at $(\epsilon_2,\gamma)=(0.34,60°)$ and 1.3 MeV higher in energy. This would be a $K=\frac{11}{2}$, oblate state. There has been discussion in the literature as to whether or not the observed 5251- or 6041-keV $\frac{11}{2}^+$ states have $K=\frac{11}{2}$;[8] we suggest that the lowest $\frac{11}{2}^+$ state corresponds to the oblate $K=\frac{11}{2}$ configuration. The 6041 keV $\frac{11}{2}^+$ is then more tentatively placed in the $[211]\frac{1}{2}$ band.

The fact that the $K=\frac{11}{2}$ state is calculated 1.3 keV above the collective $\frac{11}{2}$ state is not very surprising in view

of the general uncertainties in the CNSM calculations. Indeed, if the $s_{1/2}$ subshell were lifted so that the $[202]\frac{5}{2}$ became the ground band, this would put the collective $\frac{11}{2}$ state higher in energy but hardly influence the $K=\frac{11}{2}$ state. Thus, this state would come down in the vicinity of or maybe even below the collective $\frac{11}{2}$ state leading to a general consistency between the CNSM calculations and experiment.

### B. The 5462-keV, $\frac{13}{2}_1^+$ state

The spin parity of the $\frac{13}{2}_1^+$ state was first assigned in the mid 1970's,[7,8] and combined with previous theoretical predictions, it is considered to be $K=\frac{13}{2}$.[33,34] The lifetime has been measured as $2.5\pm1.2$ psec (Ref. 10) and the transition strength to the 3405-keV, $\frac{9}{2}^+$ ground-state band member measured as $1.1\pm0.2$ W.u. (Ref. 8) and $3.2^{+5.0}_{-2.2}$ W.u.[35] The SM results yield $\tau=1.9$ psec and $\Gamma=1.4$ W.u. These transition strengths can be compared with previously measured (present SM calculations) strengths of $7\pm4$ W.u. (Ref. 7) (8.9 W.u.) for the $\frac{9}{2}_1^+\rightarrow\frac{5}{2}_1^+$ transition and $>6$ W.u. (Refs. 6–8) (4.4 W.u.) for the $\frac{11}{2}_2^+\rightarrow\frac{7}{2}_1^+$) transition. Hence, the decay of the yrast $\frac{13}{2}^+$ state is hindered when compared to $K=\frac{5}{2}$ in-band transitions. On the other hand, if we assume $K=\frac{13}{2}$, a $\Delta K=4$ transition to the $K=\frac{5}{2}$ ground-state band would imply an even weaker strength than observed. This in turn implies that $K$ mixing is occurring in the $K=\frac{13}{2}^+$ band head and/or in the $K=\frac{5}{2}^+$ ground-state band.

The low relative energy of the $K=\frac{13}{2}$ state requires special stabilization of the intrinsic structure of $^{25}$Mg in this configuration. Figure 15 provides an explanation[36] for this. Using a static Nilsson potential and cranking

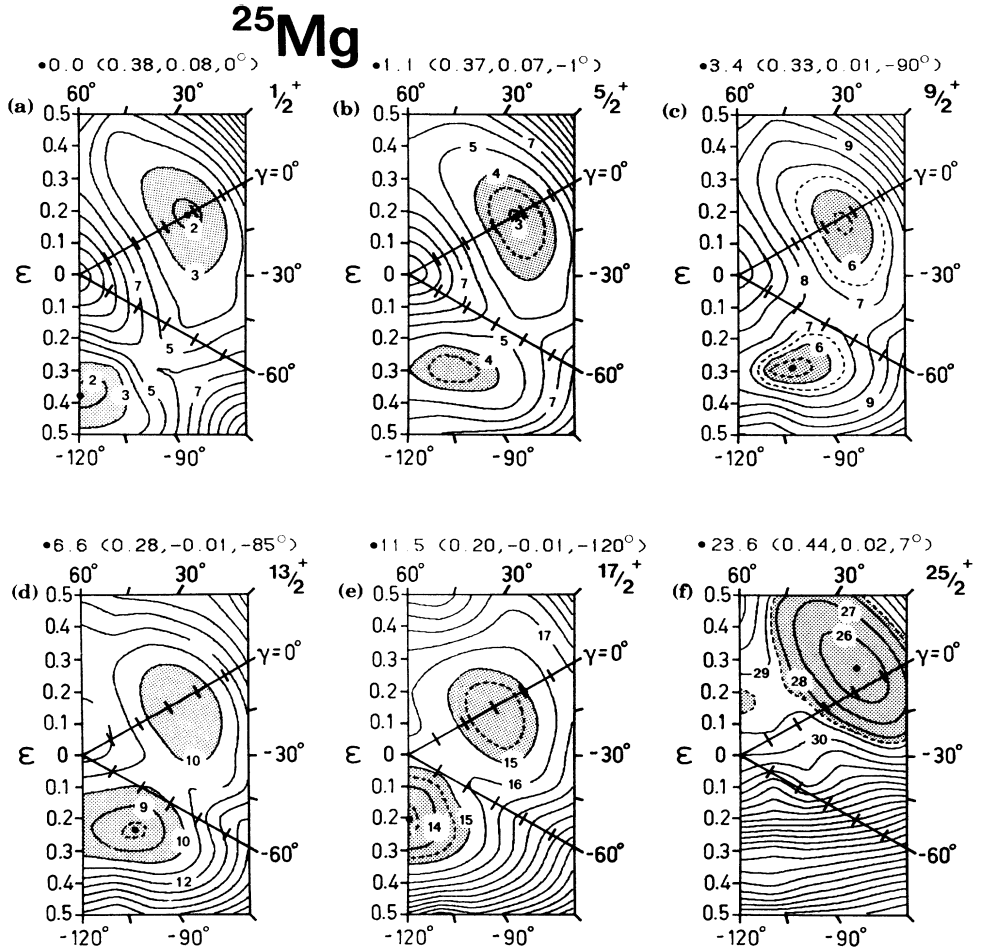


FIG. 13. Potential energy surfaces as a function of deformation for different spins in $^{25}$Mg having the configuration $(\pi,\alpha)=(+,+\frac{1}{2})$. The minimum energy in each surface is represented by a dot and the deformation at that minimum is labeled by "excitation energy" above the calculated ground state and corresponding deformation parameters, "$(\epsilon_2,\epsilon_4,\gamma)$." The ground state is calculated 1.8 MeV above the static liquid-drop energy for spherical shape which is the reference used when labeling the contour lines. Contour line spacing between solid lines is 1 MeV. The two minima in the $\frac{1}{2}^+$ surface correspond to the same state. The lowest $\frac{13}{2}^+$ minimum at $\gamma=-85°$ has a $\gamma=-120°$ edge that corresponds to a $K=\frac{13}{2}$ prolate state and is interpreted to represent the observed $\frac{13}{2}_1^+$ state at 5.46 MeV. For $J=\frac{17}{2}$, a $K=\frac{17}{2}$ prolate state is predicted to be yrast, and may represent the configuration of the observed 11 004-keV state.

around the symmetry axis, the resulting single-particle Routhians for *s-d* shell nuclei are plotted as a function of $\epsilon_2$ for $(\omega/\omega_0)/\epsilon_2=0.67$. The time-reversed degeneracy of orbitals in Fig. 12 is broken by rotation (i.e., $\pm\Omega$ orbitals) and $\epsilon_2>0$ ($<0$) corresponds to $\gamma=-120°$ (60°). Shell effects, due to different combinations of deformation and rotation, appear as gaps in energy between groups of orbitals. These gaps are labeled by particle number in circles and total spin in squares, for protons and neutrons separately. The total spin represents noncollective contributions from nucleons aligning their spins along the rotation axis.

A prolate shell gap occurs in Fig. 15 for 24 particles and a spin of 8 (neutrons plus protons). This has previously been discussed as representing the $8_1^+$ state in $^{24}$Mg.[11-13] Placing one more neutron in the prolate $[211]-\frac{3}{2}$ orbital for $\epsilon_2<0.15$ (see Fig. 15) produces a $K^\pi=\frac{13}{2}^+$ state in $^{25}$Mg at relatively low energy due to the shell effect. For $\epsilon_2>0.15$, the odd neutron enters the $[211]\frac{1}{2}$ orbital, requiring a low-lying $\frac{17}{2}^+$ state. That we can make a connection between the observed yrast $\frac{13}{2}^+$ state in $^{25}$Mg and the $8_1^+$ state in $^{24}$Mg can be seen in Fig. 13(d). In that potential energy surface, the absolute minimum appears at $(\epsilon_2,\gamma)=(0.28,-85°)$. The $\gamma=-120°$ edge of this minimum, roughly 600 keV higher in energy, corresponds to the predicted $K=\frac{13}{2}^+$ state in Fig. 15. The triaxial minimum is actually a mixture of two configurations, the first being the aligned $\frac{13}{2}^+$ state. The second configuration comes about as follows. The aligned $[211]\frac{1}{2}$ and $[211]-\frac{3}{2}$ orbitals at $\gamma=-120°$ (Fig. 15) are close-lying orbitals for an appropriate rotational frequency at the fermi surface in $^{25}$Mg, one or the other of which is filled to create the $K=\frac{13}{2}^+$ or $\frac{17}{2}^+$ states. As these orbitals move into the $\gamma$ plane towards $\gamma=-85°$, they mix together with a resultant $\frac{13}{2}^+$ state being roughly a 50:50 admixture of the two configurations. Small changes in the single-particle CNSM parameters can bring down the $\gamma=-120°$ configuration to become yrast. It, therefore, seems quite reasonable to interpret the observed $\frac{13}{2}^+$ state as being mainly of aligned character. The large overlap between the $\gamma=-120°$ and $-85°$ minima makes it improbable to observe both $\frac{13}{2}^+$ states close in energy as predicted.

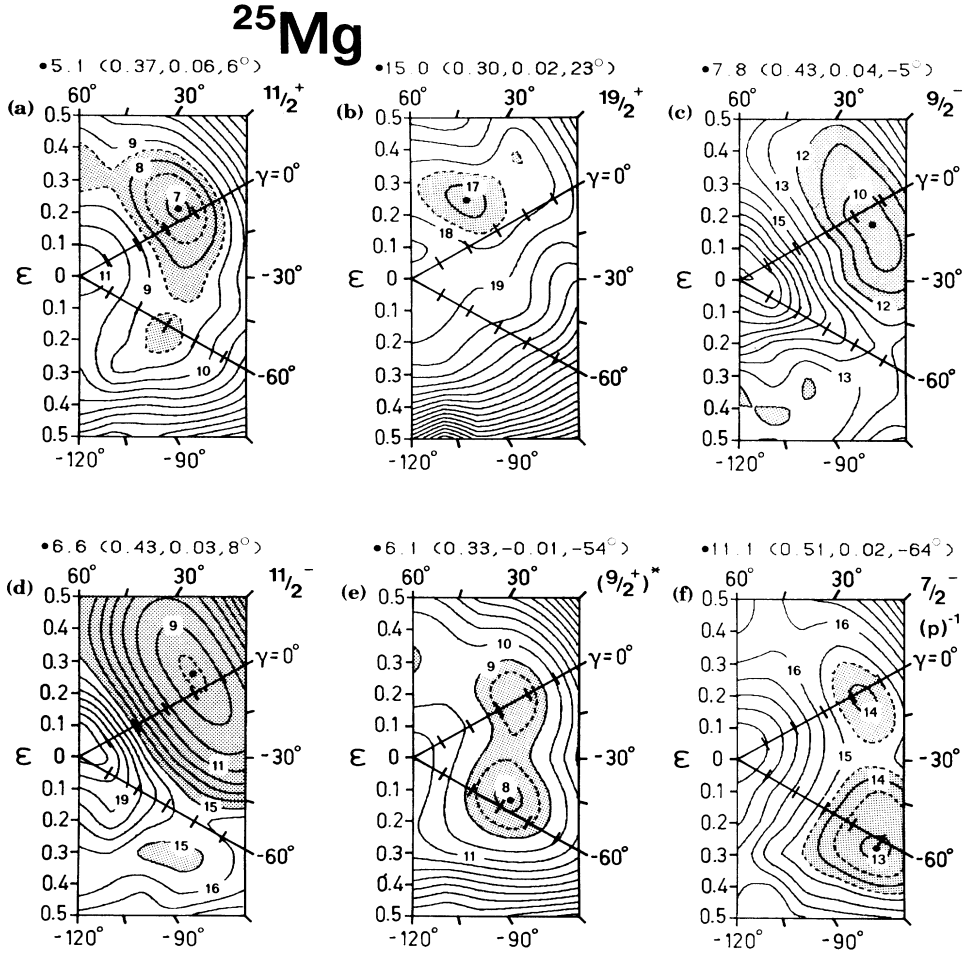


FIG. 14. Potential-energy surfaces in $^{25}$Mg as in Fig. 13. (a) and (b) $(\pi,\alpha)=(+,-\frac{1}{2})$ yrast configurations for $J=\frac{11}{2}$ and $\frac{19}{2}$. (c) and (d) Negative-parity yrast potential-energy surfaces for the $\nu(f_{7/2})$ configuration for $J=\frac{9}{2}$ and $\frac{11}{2}$. (e) $J=\frac{9}{2}$ surface for the one-hole configuration corresponding to $[211]\frac{3}{2}$ and $[200]\frac{1}{2}$ rotational bands, for prolate ($\gamma=0°$) and oblate ($\gamma=-60,$) deformations, respectively. (f) $J=\frac{7}{2}$ surface for the lowest-*p*-shell excitation in $^{25}$Mg.

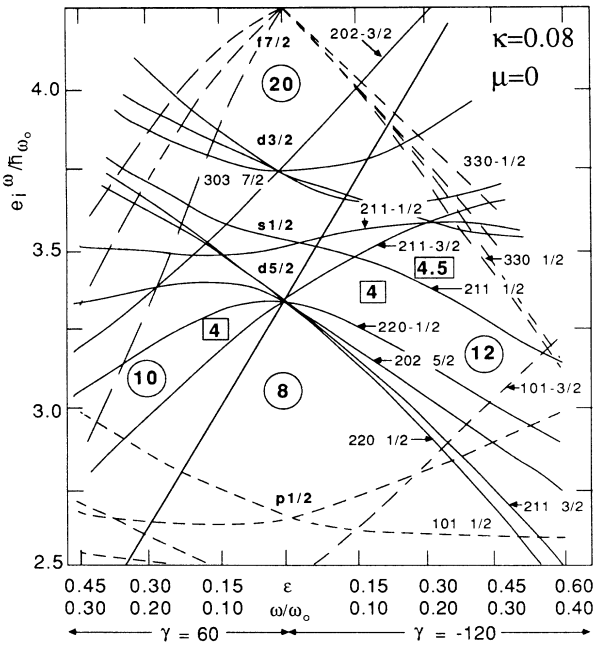


FIG. 15. Single-particle Routhians in the *s-d* shell for a Nilsson potential cranked around its symmetry axis, with $(\omega/\omega_0)/\epsilon_2=0.67$. Encircled numbers represent total particles, and numbers inside rectangles refer to total spin. Shell gaps due to different combinations of deformation and rotation predict prolate-aligned states with $K^\pi=8^+(^{24}\mathrm{Mg})$, $\frac{13}{2}^+$ and $\frac{17}{2}^+(^{25}\mathrm{Mg})$, and $4^+(^{26}\mathrm{Mg})$.

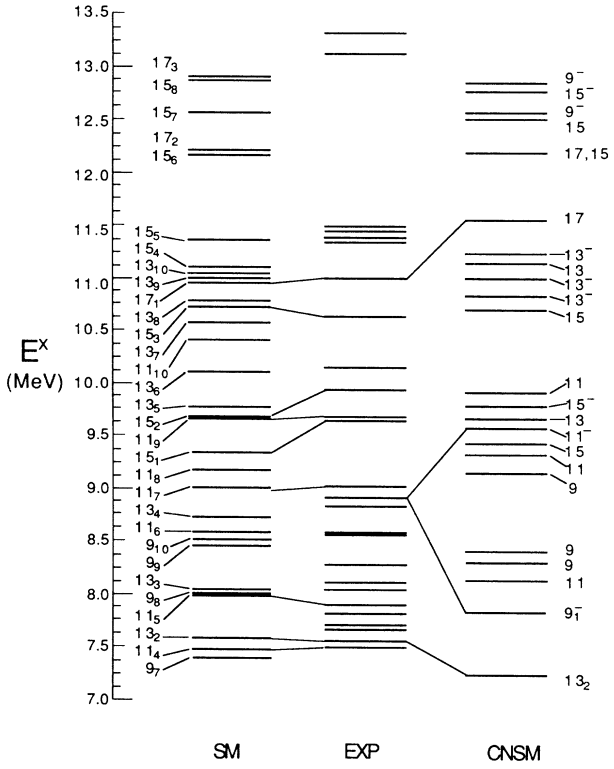


FIG. 16. Comparison of the level energies calculated in the shell model (SM) and cranked Nilsson-Strutinsky model (CNSM) with experiment for states between 7 and 13.5 MeV in $^{25}$Mg, for $J\geq\frac{9}{2}$. The low level density in the CNSM calculations is due to the fact that only selective rotational bands and particle-hole states have been considered. Comparison between some of the states in the theories and experiment is shown with a connecting line.

### C. States above 6.1 MeV; continuation of rotational bands

For comparison purposes, the situation is different for higher-spin states. The density of states decreases as $J$ increases, and pairing should completely disappear, so that both models become very useful in predicting energies, spins, and deformations of levels. Figure 16 presents a comparison of the SM and CNSM with experiment for newly observed states between 7 and 13.5 MeV. In Sec. V C1–V C 5 below we will discuss specific states and their interpretations.

The major motivation for studying high-spin states in $^{25}$Mg was to locate the $\frac{13}{2}^+$ member of the ground-state band. This would solidify the comparison of the $\frac{13}{2}^+_1$ and $\frac{13}{2}^+_2$ states in analogy with the $8^+_1$ and $8^+_2$ states in $^{24}$Mg. However, there is some question as to the validity of assigning states to particular bands above $J=\frac{9}{2}$ in $^{25}$Mg. Previous SM calculations by Cole *et al.*[33] suggest that the $(K=\frac{5}{2})$ $\frac{9}{2}^+$ state at 3405 keV contains roughly $\frac{1}{3}$ of the $K=\frac{9}{2}$ wave function at 4060 keV. One of us[37] has studied the rotational structure of $^{25}$Mg based on the sign and magnitude of $Q_0$ as well as $B(E2)$ values, the result also being that the $K=\frac{5}{2}$ band is not well established even at $J=\frac{9}{2}$. Using subshell occupancies for a given state, where $N_{d5/2}+N_{d3/2}+N_{s1/2}=9$ for $^{25}$Mg and $N_i$ is the number of nucleons on the $i$th subshell, Watt *et al.*[34] have suggested that rotational properties will disappear in $^{25}$Mg at $J=\frac{13}{2}$. Since the *s-d* SM does not allow occupation of orbitals from other shells, it seems probable that, particularly for the higher-spin states, there will be a tendency to underestimate band continuity which will shift gradually toward increased occupation of orbitals from higher shells. Indeed, in the CNSM calculations, the rotational bands can be followed (with continuously changing configurations) to their terminations for spins $J\geq 10$. In any case, in the present work we have suggested extensions of rotational bands by comparison with the relative SM $B(E2)$ strengths for $J\rightarrow(J-2)$ transitions.

#### 1. Tentative $\frac{11}{2}^+$ states

*a. The 7493-keV state.* Experimentally we have narrowed down $J$ for the 7493-keV state to be $\frac{9}{2}$, $\frac{11}{2}$, or $\frac{13}{2}$. The SM predicts the $\frac{9}{2}^+_7$, $\frac{11}{2}^+_4$, and $\frac{13}{2}^+_2$ states to lie at 7380, 7462, and 7548 keV, respectively. Based on the branching ratios and correspondence of $\frac{13}{2}^+_2$ with the observed 7550-keV state (see below and Table II), we have tentatively assigned $\frac{11}{2}^+$ to the 7493-keV state.

*b. The 7866-keV state.* We have tentatively assigned $J^\pi=(\frac{7}{2}-\frac{11}{2})^+$ or $\frac{9}{2}^-$ to this state. The SM predicts (Fig. 16) the $\frac{11}{2}{}_5^+$ and $\frac{9}{2}{}_8^+$ states to lie near this level, as well as four states with $J^\pi=\frac{7}{2}^+$ between 7.63 and 8.17 MeV. The $\frac{11}{2}{}_5^+$ SM state corresponds better than $\frac{9}{2}{}_8^+$ with the $\gamma$-ray branching ratios from the observed state; no SM calculated $\gamma$-decay from $\frac{7}{2}^+$ states is available for comparison with experiment. However, observed decay to $\frac{11}{2}$ and $\frac{9}{2}$ states and no decays to $\frac{5}{2}$ states suggests that the 7866-keV state does not have $J=\frac{7}{2}$. Assigning $\frac{11}{2}^+$ to the 7866-keV state places it energetically in the region where the $\frac{11}{2}$ member of the $[200]\frac{1}{2}$ rotational band is expected. However, no decays were observed to the $\frac{7}{2}^+$ and $\frac{9}{2}^+$ members of this band at 5012 and 5971 keV, respectively.

*c. The 9013-keV state.* With branches to the $\frac{9}{2}{}_3^+$ and $\frac{11}{2}{}_1^+$ states, we have experimentally narrowed down the spin of the 9013-keV state to $(\frac{11}{2},\frac{13}{2})^+$. Of the three close-lying $\frac{11}{2}$ and $\frac{13}{2}$ SM states (Fig. 16), the $\frac{11}{2}{}_7^+$ state, calculated to lie only 10 keV below the observed energy, emulates experiment in the two largest decay branches (Table II). The $\frac{11}{2}{}_8^+$ SM state is calculated to decay with a 59% branch to the $\frac{9}{2}{}_3^+$ state, but decays more strongly to $\frac{11}{2}{}_2^+$ and $\frac{9}{2}{}_1^+$ than to $\frac{11}{2}{}_1^+$. We, therefore, suggest the assignment of $\frac{11}{2}{}_7^+$ for the 9013-keV state.

*d. The 9685-keV state.* We have tentatively assigned $J^\pi=(\frac{11}{2},\frac{13}{2})^+$ to the 9685-keV state. The SM predicts the $\frac{11}{2}{}_{8,9}^+$ and $\frac{13}{2}{}_{5,6}^+$ states to lie within $\pm 519$ keV of this state. The observed decay branches of 63% to $\frac{9}{2}{}_1^+$ and 37% to $\frac{11}{2}{}_2^+$ do not correspond very well with the $\frac{11}{2}{}_8^+$, $\frac{13}{2}{}_5^+$, or $\frac{13}{2}{}_6^+$ decay branches. No calculation of decay branches was available for the $\frac{11}{2}{}_9^+$ SM state simply because of the lack of available wave functions for the ninth state of spin $\frac{11}{2}$. We can, however, make a very tentative assignment of $\frac{11}{2}^+$ to the observed 9685-keV state based on the process of elimination.

### 2. *The 7550-keV state and rotational coexistence in $^{25}$Mg*

A spin of $\frac{13}{2}^+$ has been assigned to the 7550 keV state. The SM calculations confirm this assignment since a $\frac{13}{2}^+$ state is predicted at 7548 keV whose decay branches are quite similar to those of the observed 7550-keV level. With two branches to the $K=\frac{5}{2}$ rotational band and $E(\frac{13}{2})$ predicted to lie at 7545 keV based on the rotational systematics for $K=\frac{5}{2}$, the 7550-keV level has the properties expected for the $\frac{13}{2}^+$ member of the ground-state band.

The SM also predicts this state to belong to the $K=\frac{5}{2}$ band. The transition strength to the $(K,J)=(\frac{5}{2},\frac{9}{2})$ state is 11.6 W.u., or 8.3 times that of the $\frac{13}{2}{}_1^+\rightarrow\frac{9}{2}{}_1^+$ decay and analogous to the situation in $^{24}$Mg, where $\Gamma(8_2^+\rightarrow 6_1^+)/\Gamma(8_1^+\rightarrow 6_1^+)=10.3$. Unlike in $^{24}$Mg, however, the 7550-keV state decays outside of the ground band with its strongest branch to the $\frac{11}{2}{}_1^+$ state. The latter decay suggests $K$ mixing as expected for the triaxial CNSM $13/2_1^+$ state.

Finally it should be noted that in Fig. 13(d), the collective minimum at $(\epsilon_2,\gamma)=(0.34,-3°)$ for the $\frac{13}{2}^+$ state corresponds to the ground-state band member. We have, therefore, in very close analogy with $^{24}$Mg, a second example in the lowest two $\frac{13}{2}^+$ states in $^{25}$Mg of rotational coexistence—two prolate states, one collective and one single particle, which differ in their axes of rotation. Further insight into the different intrinsic properties of the two sets of rotationally coexisting states can be obtained by comparing the SM subshell occupancies, $N_{5/2}$,$N_{3/2}$, and $N_{1/2}$, for the two $8^+$ states in $^{24}$Mg and the two $\frac{13}{2}^+$ states in $^{25}$Mg. This comparison is shown in Table V along with a comparison of the $\epsilon_2$ values calculated in both models. Results of the CNSM and SM formalisms of Ref. 12 are also listed for $^{24}$Mg. What is apparent in Table V is (a) the relatively large contribution of the $d_{5/2}$ subshell to the lower-energy aligned $8^+$ and $\frac{13}{2}^+$ wave functions, and (b) the smaller deformation of the aligned states. The Nilsson configuration for a prolate $K^\pi=\frac{13}{2}^+$ state (Fig. 15), $\pi[202]\frac{5}{2}$, $[211]\frac{3}{2}$, $\nu[202]\frac{5}{2}$, $[211]\frac{3}{2}$, $[211]-\frac{3}{2}$, can also be represented as

$$[\pi(d_{5/2})_4^{-2}\nu(d_{5/2})_{5/2}^{-1}]_{13/2}$$

relative to a core of 28 particles with $d_{5/2}$ fully occupied. This illustrates what has been termed the "condensation into the $d_{5/2}$ subshell" of the aligned configurations.

More generally, it seems that the low-lying $\frac{13}{2}^+$, $\frac{11}{2}^+$, and $\frac{9}{2}^+$ states which do not belong to the $[211]\frac{1}{2}$ or $[202]\frac{5}{2}$ bands can be described as members of a $(d_{5/2})^{-3}$ multiplet with a broken-pair proton configuration. On the other hand, the deformations which result are fairly large which means that the $d_{5/2}$ orbitals are rather strongly mixed. As discussed above, the maximum spin within this configuration is $\frac{13}{2}$ leading to the prolate $K=\frac{13}{2}$ state. Similarly, for signature $\alpha=-\frac{1}{2}$, the maximum spin is $\frac{11}{2}$. However, the polarizing effect is so large that the $K=\frac{11}{2}$ state becomes oblate [see discussion above and Fig. 14(a)]. For $I=\frac{9}{2}$ on the other hand, no favored $K$ state can be formed in the $(d_{5/2})^{-3}$ multiplet for either prolate or oblate shape [the lowest $K=\frac{9}{2}$ state in the present calculations is formed as $\pi[211]\frac{3}{2}^{-1}$, $[202]\frac{5}{2}\nu[211]\frac{1}{2}$; see Figs. 12 and 13(c)]. Instead a somewhat collective $\frac{9}{2}$ state is formed in $(d_{5/2})^{-3}$ leading to the triaxial minimum $(\gamma=-90°)$ in Fig. 13(c). Thus, in this interpretation, it is questionable to refer to the second $\frac{9}{2}^+$ state (observed at 4060 keV) as pure in $K$. Rather it could be considered as part of a band terminating in the $K=\frac{13}{2}$ state [or simply as belonging to a disturbed $(d_{5/2})^{-3}$ multiplet]. As the $(d_{5/2})^{-3}$ configuration contains three "unpaired particles," two of which have an aligned spin close to $\frac{5}{2}$, lower-spin states than $J=\frac{9}{2}$ are not easily formed. This provides a natural explanation why no corresponding $I=\frac{7}{2}$, etc. states are observed.

TABLE V. Subshell occupancies for the $d_{5/2}$, $d_{3/2}$, and $s_{1/2}$ subshells, and $\epsilon_2$ deformations for the rotationally coexisting states in $^{24,25,26}$Mg. All shell-model results are present results unless otherwise noted.

| Nucleus | $K^\pi$ | $J_\#$ | $(N_{5/2},N_{3/2},N_{1/2})$ | | $\epsilon_2$ | |
|---|---|---|---|---|---|---|
| | | | CNSM | SM | CNSM | SM |
| $^{24}$Mg | $8^+$ | $8_1$ | (6.89,0.21,0.76) | (7.11,0.54,0.35)[a] | 0.21[a] | 0.16 |
| | | | | (6.98,0.53,0.49) | | |
| | $0^+$ | $8_2$ | (5.40,0.96,1.22) | (6.10,1.13,0.07)[a] | 0.33[a] | 0.23 |
| | | | | (5.76,0.87,1.37) | | |
| $^{25}$Mg | $\frac{13}{2}^+$ | $\frac{13}{2}_1$ | (7.88,0.20,0.78) | (7.78,0.67,0.55) | 0.22 | 0.23 |
| | $\frac{5}{2}^+$ | $\frac{13}{2}_2$ | (6.04,0.97,1.69) | (6.76,1.25,0.98) | 0.34 | 0.33 |
| | $\frac{17}{2}^+$ | $\frac{17}{2}_1$ | (7.21,0.42,1.26) | (7.11,0.89,1.00) | 0.20 | 0.26 |
| | $(\frac{5}{2}^+)$ | $\frac{17}{2}_2$ | | (7.01,1.25,0.74) | 0.31 | 0.02 |
| | $(\frac{5}{2}^+)$ | $\frac{17}{2}_3$ | (5.83,1.22,1.67) | (5.99,1.18,1.83) | 0.31 | 0.37 |
| $^{26}$Mg | $4^+$ | $4_1$ | | (8.24,0.91,0.85) | | 0.03 |
| | $0^+$ | $4_2$ | | (7.59,1.33,1.09) | | $-3\times10^{-3}$ |

[a]Reference 12.

### 3. *The $J=\frac{15}{2}$ states*

*a. The 9650-keV state.* With an observed 100% branch to the $\frac{13}{2}_1^+$ state, the range of spins determined for the 9650-keV state is $\frac{11}{2}$ to $\frac{17}{2}$. The lowest $\frac{17}{2}^+$ state predicted in either model is above 11 MeV, which argues against this spin. Furthermore, the angular distribution of the transition decaying from the 9650-keV state to the $\frac{13}{2}^+$ 5462-keV state does not suggest a stretched $E2$ decay. In Fig. 16 it can be seen that the SM predicts the $\frac{11}{2}_9^+$, $\frac{15}{2}_{1,2}^+$, and $\frac{13}{2}_5^+$ states to lie within 400 keV of the observed state. Furthermore, we have successfully matched the calculated SM $\frac{11}{2}_9^+$ and $\frac{15}{2}_2^+$ states with experimentally observed states at 9685 and 9949 keV, respectively. The $\frac{13}{2}_5^+$ SM state decays very weakly to the $\frac{13}{2}_1^+$ state, and strongly to the $\frac{11}{2}_2^+$ (57%), $\frac{11}{2}_i^+$ (18%), and $\frac{11}{2}_3^+$ (16%) states. The calculated yrast $\frac{15}{2}^+$ SM state at 9326 keV and the $\frac{13}{2}_6^+$ SM state at 10 088 keV both decay most strongly to the $\frac{13}{2}_1^+$ state (87% and 67%, respectively). Closer correspondence in energy with the $\frac{15}{2}_1^+$ state and the tentative assignment of $\frac{15}{2}_2^+$ and $\frac{15}{2}_3^+$ to other states has led us to make the assignment of $\frac{15}{2}_1^+$ to the 9650-keV state.

The CNSM predicts the $\frac{15}{2}_1^-$ state, belonging to the $\nu[330]\frac{1}{2}$ rotational band, to lie at 9.76 MeV (see Fig. 16). Decay only to a positive-parity state, however, argues against negative parity for the 9650-keV state.

In the CNSM the $\frac{15}{2}_1^+$ state is predicted to be the collective ground-state band member and is associated with the observed 9949-keV state (see Sec. V C 3 *b*). The similarity of the quadrupole moments $Q_0$ of the $\frac{11}{2}_2^+$ and $\frac{15}{2}_3^+$ SM states to those of other states in the ground-state band (gsb) makes them the most likely members of the gsb. However, the $B(E2)$ values for decay to other gsb members are greatest for the SM yrast $\frac{11}{2}^+$ and $\frac{15}{2}^+$ states. Thus in the SM the $J^\pi(9650\text{ keV})=\frac{15}{2}^+$ state is not considered to be part of any band. One possibility is that the 9650-keV state is the $\frac{15}{2}^+$ member built on the $K=\frac{13}{2}$ state at 5462 keV. A rotational state built on the $K=\frac{13}{2}$ band head is in principle formed by a collective rotation vector that is perpendicular to the spin vector of the $K$ state. In the CNSM, it is assumed that the entire spin vector is aligned along one axis (one-dimensional cranking). Thus, a $\frac{15}{2}$ state cannot be generated in this manner. On the other hand, Leander has calculated[38,39] the $\frac{15}{2}$ member of such a high-$K$ state to lie at only 8.16 MeV in excitation for all $\epsilon_2$ deformations between 0.15 and 0.55 using the RPA. Inclusion of $\epsilon_4$ deformations reduces the energy even further. Another $\frac{15}{2}^+$ state is formed as a pure $K$-aligned prolate state with the configuration

$$[(\pi d_{5/2})_4^{-2}(\nu d_{5/2})_4^{-2}(s_{1/2})_{-1/2}]_{15/2}$$

in close correspondence to the aligned $K=\frac{17}{2}$ state discussed below. It is calculated at an excitation energy of 10.8 MeV and a deformation of $(\epsilon_2,\gamma)=(0.2,-120°)$.

*b. The 9949- and 10 653-keV states.* Agreement between experiment and theory is good when $J^\pi=\frac{15}{2}^+$ is assigned to both the 9949 and 10 653-keV states (see Table II). Using 7550 keV as the energy of the $(K,J)=(\frac{5}{2},\frac{13}{2})$ state, an energy of 9873 keV is predicted for the $\frac{15}{2}^+$ member of the $K=\frac{5}{2}^+$ band. If the 9949-keV state were part of the ground band, its decay to the yrast $\frac{11}{2}^+$ and $\frac{13}{2}^+$ states would indicate considerable wave-function mixing, as already noted for the $\gamma$ decays of 7550 $\frac{13}{2}^+$ state. The 10 653-keV state is experimentally observed to decay only to the $\frac{11}{2}^+$ and $\frac{13}{2}^+$ members of the $K=\frac{5}{2}$ band. This suggests that it is the $\frac{15}{2}^+$ member of the $K=\frac{5}{2}$ rotational band. The calculated $B(E2)$ values for decays from the $\frac{15}{2}_3^+$ state to the $\frac{11}{2}_{1,2,3}^+$ states are in the ratio 1:112:36. For the $\frac{15}{2}_2^+$ the ratios are 1:0.03:1.3. The predicted $Q_0$ for the $\frac{15}{2}_3^+$ ($\frac{15}{2}_2^+$) state (assuming $K=\frac{5}{2}$ for conversion into a rotating frame) is 33.2 (25.9) compared to SM $Q_0$ values of 48.4, 92.9, $-18.6$, 41.0, and 52.4 for the $(K=\frac{5}{2})\frac{13}{2}$, $\frac{11}{2}$, $\frac{9}{2}$, $\frac{7}{2}$, and $\frac{5}{2}$ states, respectively. There-

fore, the SM tentatively suggests that the $\frac{15}{2}_3^+$ state observed at 10 653 keV belongs to the $K=\frac{5}{2}$ band, although the alternative $\frac{15}{2}_2^+$ state cannot be completely excluded.

The CNSM predicts the lowest-lying collective $\frac{15}{2}^+$ state to lie at 9.4 MeV, with $[\epsilon_2,\epsilon_4,\gamma]=[0.34,0.05,12°]$. This we associate with the 9949-keV observed state, with no correspondence to the observed 10 653-keV state since two $(+,+\frac{1}{2})$ rotational bands are not generated in the present CNSM calculations. On the other hand, considerations based on the CNSM suggest at least four relatively low-lying $\frac{15}{2}^+$ states, namely the collective ones belonging to the $[202]\frac{5}{2}$ and $[211]\frac{1}{2}$ bands, the one built on the $K=\frac{13}{2}$ state and the aligned one with four $d_{5/2}$ holes and one $S_{1/2}$ neutron (see Sec. V C 3 *a*).

#### 4. The $J=\frac{17}{2}$ states

*a. The 11 004-keV state.* We have narrowed down the spin of the 11 004-keV state to $\frac{15}{2}^+$ or $\frac{17}{2}^+$, favoring $\frac{17}{2}^+$. As Fig. 16 shows, the SM excitations energy region between 11 and 11.5 MeV contains several high-spin states including $\frac{15}{2}^+_{4,5}$ and $\frac{17}{2}_1^+$. The energy and branching ratio of the $\frac{17}{2}_1^+$ state are in good agreement with experiment.

In Fig. 13(e), the potential energy surface for $\frac{17}{2}^+$ configurations predicts an aligned, yrast state with $(\epsilon_2,\gamma)=(0.20,-120°)$. The SM gives $\epsilon_2=0.26$ for this state (Table V). The $\frac{17}{2}^+$ ground-state band member in Fig. 13(e) lies 660 keV higher in energy with $(\epsilon_2,\gamma)=(0.31,-3°)$. These two calculated $\frac{17}{2}$ states, then, make up the second pair of rotationally coexisting states in $^{25}$Mg.

The $B(E2)$ strength calculated with the SM for the $\frac{17}{2}_1^+\rightarrow\frac{13}{2}_2^+$ transition is 1140 times smaller than that of the $\frac{17}{2}_2^+\rightarrow\frac{13}{2}_2^+$ transition, where the $\frac{17}{2}_2^+$ state is a member of the ground-state rotational band. This relative reduction in strength, assuming that the yrast SM and CNSM $\frac{17}{2}^+$ states correspond to each other, is even more pronounced than the calculated $(\frac{13}{2}_1\rightarrow\frac{9}{2}_1)/(\frac{13}{2}_2\rightarrow 9/2_1)$ ratio or the observed $(8_1^+\rightarrow 6_1^+)/(8_2^+\rightarrow 6_1^+)$ ratio in $^{24}$Mg. Furthermore, the $B(E2)$ strength for the $\frac{17}{2}_1^+\rightarrow\frac{13}{2}_1^+$ transition is predicted to be 260 times greater than that of the $\frac{17}{2}_1^+\rightarrow\frac{13}{2}_2^+$ transition in the SM calculations, indicating strong relative overlap of the yrast states. The observed state at 11 004 keV in $^{25}$Mg is thus tentatively assigned as a $K^\pi=\frac{17}{2}^+$ state because of its close correspondence to the yrast SM state in energy and $\gamma$ decay, and because of the deformation of this yrast state predicted by the CNSM. It is also interesting to note that the $B(E2)$ values calculated in the shell model seem to indicate that the $\frac{17}{2}_1$ state is a more pure "$K$ isomer" than the $\frac{13}{2}_1$ state, in qualitative agreement with the more pronounced CNSM $\gamma=-120°$ minimum for $\frac{17}{2}$ than for $\frac{13}{2}$.

*b. The 11 410- and 13 332-keV states.* The observed state at 11 410 keV is a candidate for the second $\frac{17}{2}^+$ state, which would complete our identification of the rotational pairs in $^{25}$Mg. In Table V, the subshell occupancies again indicate that for the yrast $\frac{17}{2}^+$ state, a relatively large $d_{5/2}$ occupation is expected. Both the $\frac{17}{2}_2^+$ state and the $\frac{17}{2}_3^+$ state at 13 332 keV are listed in Table V because, while relative $B(E2)$ strengths to the $(K,J)=(\frac{5}{2},\frac{13}{2})$ state at 7550 keV strongly favor the assignment of the $\frac{17}{2}_2^+$ state to the ground-state band, the subshell occupancies and calculated $Q_0$ values favor $\frac{17}{2}_3^+$.

The CNSM predicts the $\frac{17}{2}_1^+$ state to be the terminating state in a band including lower-spin members. Similar considerations were expected for the $\frac{13}{2}^+$ potential energy surface of Fig. 13(d). This concept is in keeping with the observed effect of rotation on deformation. In general, at the beginning of a shell, configurations evolve from collective prolate shapes ($\gamma=0°$) through the $\gamma$ plane partially or completely to oblate aligned states at $\gamma=60°$, while at the end of a shell the evolution is from collective oblate ($-60°$) towards noncollective prolate shapes ($-120°$).[40] (The latter case of rotation around the long axis is unfavored from a classical standpoint; for $^{25}$Mg in the CNSM, the macroscopic energy for $\epsilon_2=0.2$ and $J=\frac{17}{2}$ favors an oblate over a prolate shape by roughly 3.5 MeV.) Thus, four holes in the $d_{5/2}$ subshell can give a band terminating at $8^+$ in $^{24}$Mg, and four $d_{5/2}$ holes coupled with one $s_{1/2}$ particle or hole would predict a band terminating at $\frac{17}{2}^+$ for $^{25}$Mg.

#### 5. Possible negative-parity states

While negative-parity states are not included in the SM configuration space for $^{25}$Mg, they are readily calculated in the CNSM.

Figures 14(c) and 14(d) display the potential-energy surfaces for yrast configurations in $^{25}$Mg with $J^\pi=\frac{9}{2}^-$ and $\frac{11}{2}^-$. The $\nu[330]\frac{1}{2}$ rotational band is predicted to be yrast for negative-parity states through $J=\frac{11}{2}$. Most of the members of this band have been observed previously. Only new negative-parity states will be discussed here.

*a. The 8895-keV state.* The previously unobserved $\frac{9}{2}^-$ member of the $\nu[330]\frac{1}{2}$ rotational band is predicted in Fig. 14(c) to lie at 7.8 MeV, with $(\epsilon_2,\gamma)=(0.43,-5°)$. The spin of the 8895-keV state has been assigned $(\frac{9}{2},\frac{11}{2})^-$. If $J(8895)=\frac{9}{2}$, it should almost certainly be assigned as the $\frac{9}{2}^-$ member of the $K^\pi=\frac{1}{2}^-$ yrast band.

*b. The 11 361- and 13 143-keV states.* The 11 361- and 13 143-keV states have been tentatively assigned $(\frac{13}{2},\frac{15}{2})^-$ and $(\frac{11}{2}-\frac{15}{2})^-$; $\frac{13}{2}^+$, respectively. As shown in Fig. 16, using the CNSM we calculate several $\frac{13}{2}^-$ states and one $\frac{15}{2}^-$ state between 10.8 and 12.8 MeV excitation. The yrast CNSM $\frac{13}{2}^-$ state at 10.9 MeV with $(\epsilon_2,\gamma)=(0.42,5°)$ represents the configuration $\nu[211]\frac{1}{2}_-$, $\pi[211]\frac{3}{2}_+^{-1}$, $[330]\frac{1}{2}_-$, where the subscripts + and − refer to the signatures $\alpha=+\frac{1}{2}$ and $\alpha=-\frac{1}{2}$, respectively. In this configuration, the favored signature of the $[330]\frac{1}{2}_-$ orbital is thus occupied, which is "compensated" by a total signature of $\alpha=1$ for the $N=2$ configuration. As the two $N=2$ orbitals $[211]\frac{1}{2}$ and $[211]\frac{3}{2}$ are essentially signature degenerate (see Fig. 16 of Ref. 13), several $\frac{13}{2}^-$ states are calculated at a similar en-

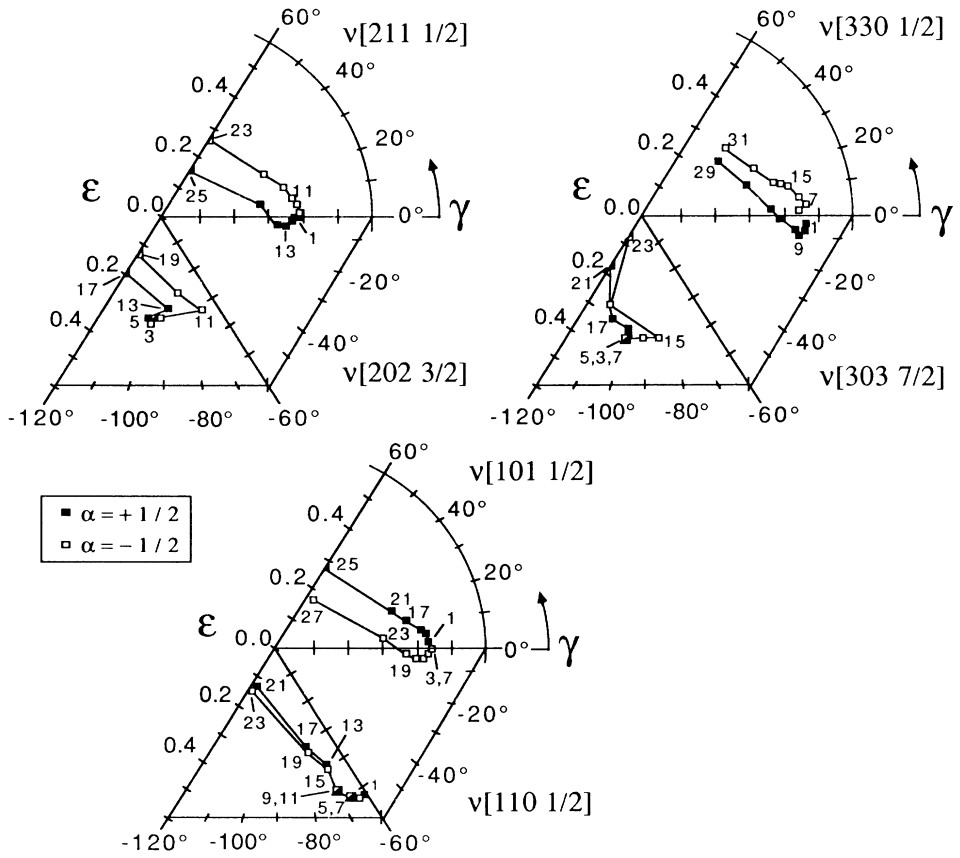


FIG. 17. Spin trajectories in the $(\epsilon_2,\gamma)$ plane for different fixed configurations in $^{25}$Mg labeled by the appropriate Nilsson quantum number for prolate or oblate shape, respectively. Rotational bands are separated according to signature, with spins labeled by $2J$. Sequences of spins whose deformation remains in the same sector (or nearly so) are grouped together. The bands for which experimental counterparts have been found are seen to evolve from prolate collective deformations through the $\gamma$ plane to oblate or near-oblate terminations.

ergy (if no symmetrization is performed). Furthermore, the $\frac{13}{2}^-$ state of the unfavored signature branch of the $[330]\frac{1}{2}$ band is calculated to lie at 11.23 MeV with $(\epsilon_2,\gamma)=(0.42,-4°)$. The excitation energy of this latter, $[330]\frac{1}{2}_+$ state is only 130 keV below the observed 11 361-keV state, but the association remains tentative without a definite spin assignment. A CNSM state at 12.78 MeV in Fig. 16, with $J^\pi=\frac{15}{2}^-$, results from the configuration $\nu[211]\frac{1}{2}$ $\pi[211]\frac{3}{2}^{-1}$ $[330]\frac{1}{2}$, where again the favored signature branch of the $[330]\frac{1}{2}$ orbital is occupied while different signature combinations are possible for the $N=2$ particle-hole pair.

### D. Further aspects of the CNSM

The CNSM yields results for states of higher spin and/or excitation energy that warrant further discussion. The $\frac{19}{2}^+$ potential energy surface for yrast configurations is plotted in Fig. 14(b), where we see the $[211]\frac{1}{2}_-$ band member as a very broad absolute minimum at $\gamma=23°$. This illustrates the gradual alignment of spins for the yrast rotational band. Figure 13(f) displays the $\frac{25}{2}^+$ yrast potential energy surface, where the lowest minimum corresponds to the configuration $\nu[330]$ $\frac{1}{2}$, $\pi[211]\frac{3}{2}$, $[330]\frac{1}{2}$. The rotational band built on this particle-hole excitation is calculated to become yrast at spin $\frac{21}{2}$. At $J^\pi=\frac{25}{2}^+$, the maximum *s-d* shell spin for nine particles is reached, and the termination of the ground-state band can be seen as a secondary minimum in Fig. 13(f) at $(\epsilon_2,\gamma)=(0.17,60°)$, 2.9 MeV above the yrast $\frac{25}{2}^+$ state.

Figure 14(f) displays the $\frac{7}{2}^-$ surface for the lowest-*p*-shell excitation in $^{25}$Mg, for both prolate and oblate deformations. For $J=\frac{7}{2}$ the oblate rotational state built on the $[110]\frac{1}{2}$ intrinsic configuration is predicted to be yrast. The $\epsilon_2$ deformation of 0.51 is quite large for $^{25}$Mg.

Figure 17 displays spin trajectories as a function of deformation for four Nilsson configurations (the Nilsson labeling is valid at low spin only, due to the mixing that occurs with increasing $\omega$ in the cranking model). These diagrams are a compact way of showing how the positions of minima on potential energy surfaces change as a function of spin in a given rotational band. Most Nilsson states seen experimentally begin at prolate collective shapes and evolve towards their termination at or near $\gamma=60°$. All bands are separated according to their signature. For each diagram we see the competing oblate

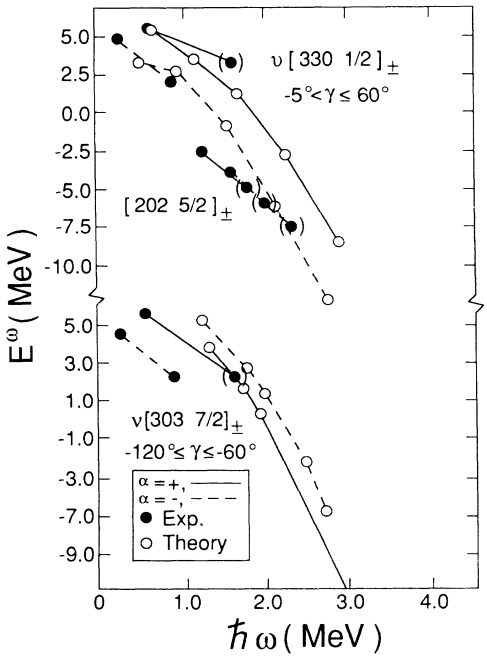


FIG. 18. Experimental Routhians for the $\nu[330]\frac{1}{2}\pm$ and $\nu[202]\ \frac{5}{2}\pm$ bands. The former are compared with calculated Routhians for the $\nu(f_{7/2})\pm$ bands determined for the $\gamma$ sectors $-5°<\gamma<60°$, $[330]\frac{1}{2}$, and $-60°<\gamma<-120°$, $[303]\frac{7}{2}$. No calculated band exists for the $[202]\frac{5}{2}$ configuration. The bands for the $[202]\frac{5}{2}$ configuration include the tentative $\frac{13}{2}$ state at 7550 keV and the $\frac{15}{2}$ states at 9949 and 10653 keV. Note the large signature splitting for the $\frac{1}{2}^-$ band compared to the ground band. The relative energy of the $\alpha=+\frac{1}{2}$ and $\alpha=-\frac{1}{2}$ curves at a given frequency is inverted for the two $\gamma$ sectors in the $\frac{1}{2}^-$ bands, and better agreement between theory and experiment exists in the positive $\gamma$ sector.

minimum at $\gamma\approx-60°$ evolving towards $\gamma=-120°$. The only candidate for such an oblate or near-oblate state is the second $\frac{9}{2}^+$ state which might be a member of a band terminating in the $K=\frac{13}{2}$ state. It should be noted, however, that all these states are expected rather high up in the spectrum where they might be strongly mixed and therefore difficult to identify in the experimental spectrum. The diagram labeled by $[101]\frac{1}{2}$ for $\gamma\geq-10°$ and $[110]\frac{1}{2}$ for $\gamma\leq-60°$ illustrates the lowest-$p$-shell excitations calculated for prolate and oblate deformations [cf. Fig. 14(f)].

Signature splitting for the experimental $[202]\frac{5}{2}\pm$ band and for the calculated and experimental $f_{7/2}$ bands is illustrated by the Routhians in Fig. 18. The $y$ axis is $E^\omega=\frac{1}{2}(E_i+E_f)-\omega J_x(J_{\rm ave})$, with $E_i$ and $E_f$, the experimental or theoretical level energies for a given band, and $J_{\rm ave}=\frac{1}{2}(J_i+J_f)$. Also,

$$J_x(J_{\rm ave})=[(J_{\rm ave}+\tfrac{1}{2})^2-K^2]^{1/2}$$

(using a rotation-aligned coupling scheme) and

$$h\omega(J_{\rm ave})=E_\gamma/[J_x(J_i)-J_x(J_f)]$$

in MeV. By plotting $E^\omega$ versus $\hbar\omega$ the difference in energy for $\alpha=\pm\frac{1}{2}$ bands at a given $\omega$ represents the signature splitting.

The $\nu f_{7/2}$ Routhians are plotted for both of the calculated rotational bands, i.e., with $\gamma\geq-5°$ and $\gamma\leq-60°$ (see Fig. 17). The data points using observed energies are plotted against both calculated bands for comparison. As expected, we see a much larger splitting for the $K^\pi=\frac{1}{2}^-$ band than for the $K=\frac{7}{2}$ band. Experiment and theory agree much better for the $K=\frac{1}{2}$ band with $\gamma\geq-0.5°$. The $[202]\frac{5}{2}$ Routhian contains both tentative $\frac{15}{2}^+$ states, at 9949 and 10653 keV, plotted for comparison. From energy systematics the 9949-keV state, with a resulting smaller increase in $\omega$ from the preceding data point, would be more likely as a part of the $K=\frac{5}{2}$ rotational band. As we have discussed above, however, the 10653-keV state is assigned to $K=\frac{5}{2}$ based on its decay modes and a comparison with SM predictions.

## VI. CONCLUSIONS

The level scheme of $^{25}$Mg is plotted in Fig. 19 as excitation energy versus $J(J+1)$. We have included all of the tentative $\frac{9}{2}$ through $\frac{17}{2}$ states in the present work, including the 8895-keV, $\frac{9}{2}^-$ (or $\frac{11}{2}^-$) state, the $\frac{11}{2}^+$ states at 7493, 7866, 9013, and 9685 keV, the $\frac{13}{2}^+$ state at 7550 keV, the three $\frac{15}{2}^+$ states at 9650, 9949, and 10653 keV, and the $\frac{17}{2}^+$ state at 11004 keV. The yrast line is plotted as $E^{\rm ex}$ versus $J$ in Fig. 20. The predicted SM energies agree quite well with the experimental ones. Except for the lowest spins, agreement between the CNSM and experiment is also good; the calculated $\frac{13}{2}_1^+$ state does not appear as favored energetically because the corresponding $\frac{9}{2}^+$ state is also favored. Both models predict the $\frac{19}{2}_1^+$ state to lie near 14 MeV, a region from which $\gamma$ decay could still be seen for such a state of this spin.

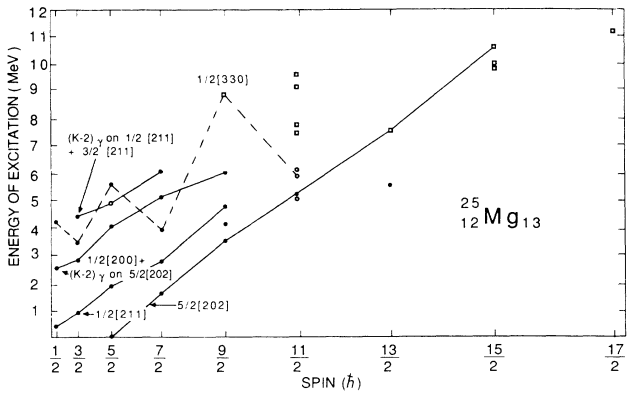


FIG. 19. Experimental band structure in $^{25}$Mg including present results, labeled by the Nilsson quantum numbers $\Omega[Nn_z\Lambda]$. ○ label tentative spins that were previously assigned, and □ identify tentative additions from this research. The $\frac{9}{2}^-$ member of the $\frac{1}{2}^-[330]$ band could also be $\frac{11}{2}^-$. Possible configuration assignments of the second $\frac{9}{2}^+$ state and of the first and fourth $\frac{11}{2}^+$ states are given in Table IV.

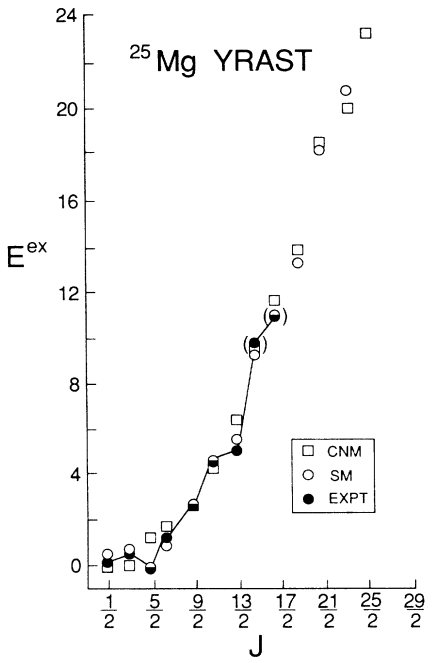


FIG. 20. Plot of the excitation energy vs spin for calculated and observed positive-parity yrast states in $^{25}$Mg, showing both SM and CNSM predictions. Tentative spins are in parentheses.

The *s-d* SM has proven very successful in reproducing energies and decay properties of most positive-parity states observed below 11 MeV in excitation energy and has provided an explanation of the $^{25}$Mg spectrum in terms of the degrees of freedom of nine active nucleons outside an inert $^{16}$O core. The CNSM complements the SM by interpreting the data in terms of the interplay of collective and single-particle degrees of freedom and by providing an interpretation of the negative-parity states and the very high-spin positive-parity states.

The phenomenon of rotational coexistence, predicted by the CNSM, has been shown to occur in $^{24}$Mg at $I^{\pi}=8^{+}$. The present work shows that this same effect can also be seen in the $\frac{13}{2}^{+}$ and $\frac{17}{2}^{+}$ states in $^{25}$Mg. The previously observed yrast $\frac{13}{2}^{+}$ state can now be interpreted as the $K=\frac{13}{2}^{+}$ aligned noncollective state since the higher $(K,J)=(\frac{5}{2},\frac{13}{2})$ state has not been found. Furthermore, we have suggested that the second $\frac{9}{2}^{+}$ state (often referred to as $K=\frac{9}{2}$) belongs to a band terminating in the $K=\frac{13}{2}$ state. The yrast $K=\frac{17}{2}^{+}$ state has also been tentatively located.

We can now expand the concept of rotational coexistence to include $^{26}$Mg. Returning to Fig. 15 for cranked Nilsson orbitals, a spin of $4\hbar$ from protons alone can be obtained in $^{26}$Mg by placing one neutron in each of the six $d_{5/2}$ orbitals. As in $^{24}$Mg and $^{25}$Mg, this provides an explanation for the physical nature of the observed $4_1^+$ state in $^{26}$Mg. It is too low in energy for inclusion in the ground-state band[41] and decays solely by an $E2$ transition to the $2_1^+$ state with a strength that is roughly four times less than the $4_2^+ \rightarrow 2_1^+$ strength. The relationship between the $4_2^+$ and $4_1^+$ states is thus very similar to that between the $8_{1,2}^+$ and $\frac{13}{2}_{1,2}^{+}$ and $\frac{13}{2}_{1,2}^{+}$ states in $^{24}$Mg and $^{25}$Mg, respectively. Table IV shows that the $d_{5/2}$ condensation and smaller deformation for the $K=4^{+}$ state, as in $^{24}$Mg and $^{35}$Mg, are signatures of this high-spin effect in light nuclei.

## ACKNOWLEDGMENTS

This research has been supported by the National Science Foundation under Grant Nos. PHY85-09736, PHY86-05032, PHY86-03874, and PHY87-18772, by the U. S. Department of Energy, Office of High Energy and Nuclear Physics under Contract No. DE-AC05-76ER01067, and by the Swedish Natural Science Research Council. We are grateful to K. W. Kemper for his assistance with the $^{14}$N beam production. Special thanks go to Tord Bengtsson for his advice and help in performing the cranking model computer calculations and to Georg Leander and Sven Åberg for specific calculations and discussion.

*Present address: Chemistry Department, Eastern Mennonite College, Harrisonburg, VA 22801.
†Present address: Department of Physics, University of Pennsylvania, Philadelphia, PA 19104.
‡Present address: Zweites Physikalisches Institut der Universität Göttingen, D-3400 Göttingen, Federal Republic of Germany.
§Present address: Physics Division, Argonne National Laboratory, Argonne, IL 60439.
**Present address: College of Arts and Sciences, University of New Mexico, Albuquerque, NM 87131.

[1]A. E. Litherland, H. McManus, E. B. Paul, D. A. Bromley, and H. E. Gove, Can. J. Phys. **36**, 378 (1958).
[2]S. G. Nilsson, K. Dan. Vidensk. Selsk. Mat. Fys. Medd. **29**, 16 (1955).
[3]R. K. Sheline and R. Harlan, Nucl. Phys. **29**, 177 (1962).
[4]D. C. Kean and R. W. Ollerhead, Can. J. Phys. **50**, 1539 (1972).
[5]H. Röpke, V. Glattes, H. J. Brundiers, and G. Hammel, Z. Phys. **260**, 67 (1973).
[6]H. Röpke, G. Hammel, W. Brendler, P. Betz, and V. Glattes, Z. Phys. **266**, 55 (1974).
[7]R. W. Ollerhead, D. C. Kean, S. G. T. Leong, C. Doekes, and T. M. R. Meadley, Can. J. Phys. **53**, 123 (1975).
[8]P. A. Butler, A. J. Brown, L. L. Green, A. N. James, C. J. Lister, J. D. MacArthur, P. J. Nolan, and J. F. Sharpey-Schafer, J. Phys. G **1**, 665 (1975).
[9]T. Kihm, G. Mairle, P. Grabmayr, K. Knopfle, G. Wagner, B. Bechtold, and L. Friedrich, Z. Phys. A **318**, 205 (1984).
[10]P. Endt and C. Van der Leun, Nucl. Phys. **A310**, 1 (1978).
[11]D. M. Headly, R. K. Sheline, S. L. Tabor, U. J. Hüttmeier, C. J. Gross, E. F. Moore, G. H. Wildenthal, H. R. Weller, R. M. Whitton, and I. Ragnarsson, Phys. Lett. **198B**, 433 (1987).

[12]R. K. Sheline, I. Ragnarsson, S. Aberg, and A. Watt (to be published).
[13]I. Ragnarsson, S. Aberg, and R. K. Sheline, Phys. Scr. **24**, 215 (1981).
[14]H. V. Klapdor, G. Rosner, H. Reiss, and M. Schrader, Nucl. Phys. **A244**, 157 (1975).
[15]K. Cordell, M. S. thesis, Florida State University, 1974.
[16]A. Litherland and A. Ferguson, Can. J. Phys. **39**, 788 (1961).
[17]A. Poletti and E. Walburton, Phys. Rev. **137**, B595 (1965).
[18]R. D. Gill, *Gamma Ray Angular Correlations* (Academic, New York, 1975), p. 1.
[19]H. J. Rose and D. M. Brink, Rev. Mod. Phys. **39**, 306 (1967).
[20]P. Taras and B. Haas, Nucl. Instrum. Methods **123**, 73 (1975).
[21]P. J. Twin, Nucl. Instrum. Methods **106**, 481 (1973).
[22]B. H. Wildenthal, Part. Nucl. Phys. **11**, 5 (1984).
[23]B. A. Brown and B. H. Wildenthal, Phys. Rev. C **28**, 2397 (1983); B. A. Brown and B. H. Wildenthal, At. Data Nucl. Data Tables **33**, 347 (1985).
[24]B. A. Brown, R. Radki, and B. H. Wildenthal, Phys. Rep. **101**, 314 (1983).
[25]B. M. Preedom and B. H. Wildenthal, Phys. Rev. C **6**, 1633 (1972).
[26]W. Chung, Ph.D. thesis, Michigan State University, 1976.
[27]A. Watt, B. Kelvin, and R. R. Whitehead, Phys. Lett. **63B**, 385 (1976).
[28]D. Branford, M. J. Spooner, and I. F. Wright, Part. Nucl. **4**, 231 (1972).
[29]G. Andersson, S. E. Larsson, G. Leander, P. Møller, S. G. Nilsson, I. Ragnarsson, S. Åberg, R. Bengtsson, J. Dudek, B. Nerlo-Pomorska, K. Pomorski, and Z. Szymanski, Nucl. Phys. **A268**, 205 (1976).
[30]T. Bengtsson and I. Ragnarsson, Nucl. Phys. **A436**, 14 (1985).
[31]C. Lederer and V. Shirley, *Table of Isotopes* (Wiley, New York, 1978), p. 46.
[32]R. Weber, B. Jeckelmann, J. Kern, V. Kiebele, B. Aas, W. Beer, I. Beltrami, K. Bos, G. deChambrier, P.F.A. Goudsmit, H. J. Leisi, W. Ruckstuhl, G. Strassner, and A. Vacchi, Nucl. Phys. **A377**, 361 (1982).
[33]B. J. Cole, A. Watt, and R. Whitehead, J. Phys. G **1**, 17 (1975).
[34]A. Watt, D. Kelvin, and R. Whitehead, J. Phys. G **6**, 35 (1980).
[35]H. Röpke, W. Brendler, P. Betz, V. Glattes, and G. Hammel, Z. Phys. **271**, 59 (1974).
[36]I. Ragnarsson, Phys. Lett. **80B**, 4 (1978).
[37]M. Carchidi and B. H. Wildenthal, Phys. Rev. C **37**, 1681 (1988).
[38]G. A. Leander, private communication.
[39]P. Arve, Y. S. Chen, and G. A. Leander, Phys. Scr. **15**, 157 (1983).
[40]C. G. Andersson, G. Hellstrom, G. Leander, I. Ragnarsson, S. Aberg, J. Krumlinde, S. G. Nilsson, and Z. Szymanski, Nucl. Phys. **A309**, 141 (1978).
[41]F. Glatz, S. Norbert, E. Bitterwolf, A. Burkard, F. Heidinger, Th. Kern, R. Lehmann, H. Röpke, J. Siefert, C. Schneider, and B. H. Wildenthal, Z. Phys. A **324**, 187 (1986).

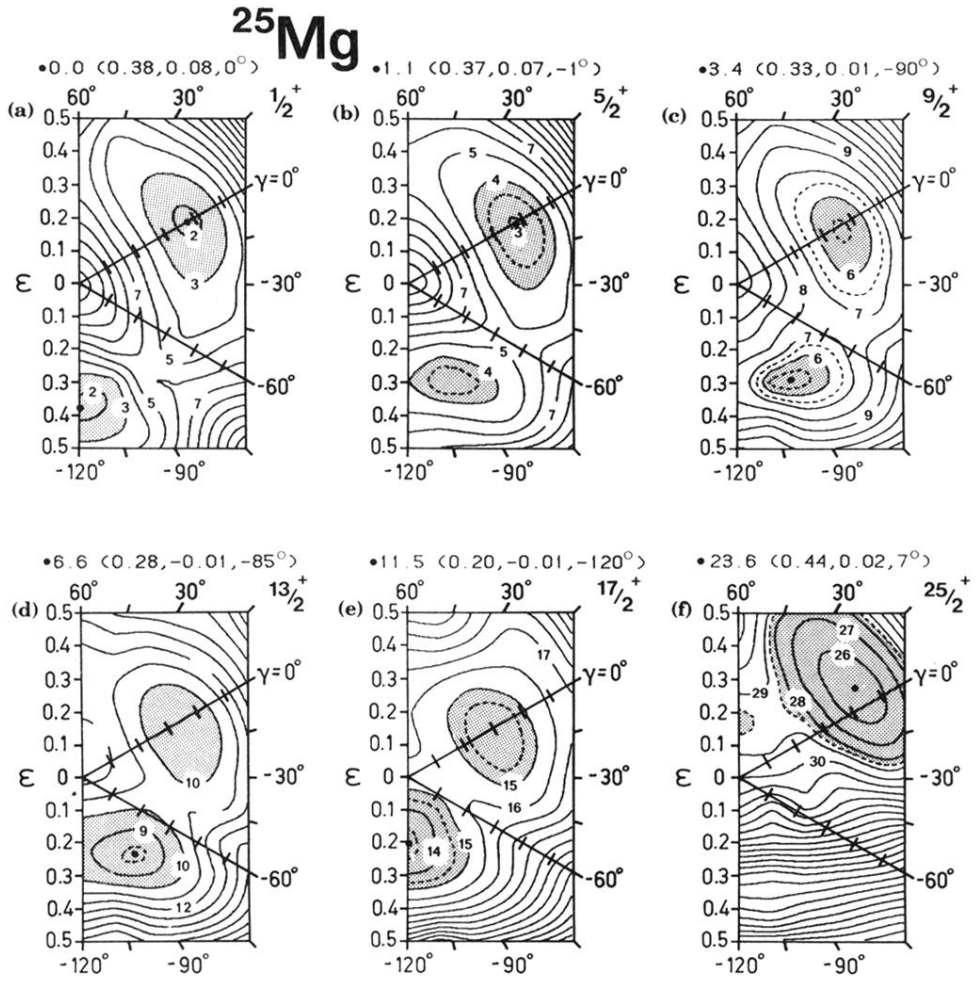


FIG. 13. Potential energy surfaces as a function of deformation for different spins in $^{25}$Mg having the configuration $(\pi,\alpha)=(+,+\frac{1}{2})$. The minimum energy in each surface is represented by a dot and the deformation at that minimum is labeled by "excitation energy" above the calculated ground state and corresponding deformation parameters, "$(\epsilon_2,\epsilon_4,\gamma)$." The ground state is calculated 1.8 MeV above the static liquid-drop energy for spherical shape which is the reference used when labeling the contour lines. Contour line spacing between solid lines is 1 MeV. The two minima in the $\frac{1}{2}^+$ surface correspond to the same state. The lowest $\frac{13}{2}^+$ minimum at $\gamma=-85°$ has a $\gamma=-120°$ edge that corresponds to a $K=\frac{13}{2}$ prolate state and is interpreted to represent the observed $\frac{13}{2}^+_1$ state at 5.46 MeV. For $J=\frac{17}{2}$, a $K=\frac{17}{2}$ prolate state is predicted to be yrast, and may represent the configuration of the observed 11 004-keV state.

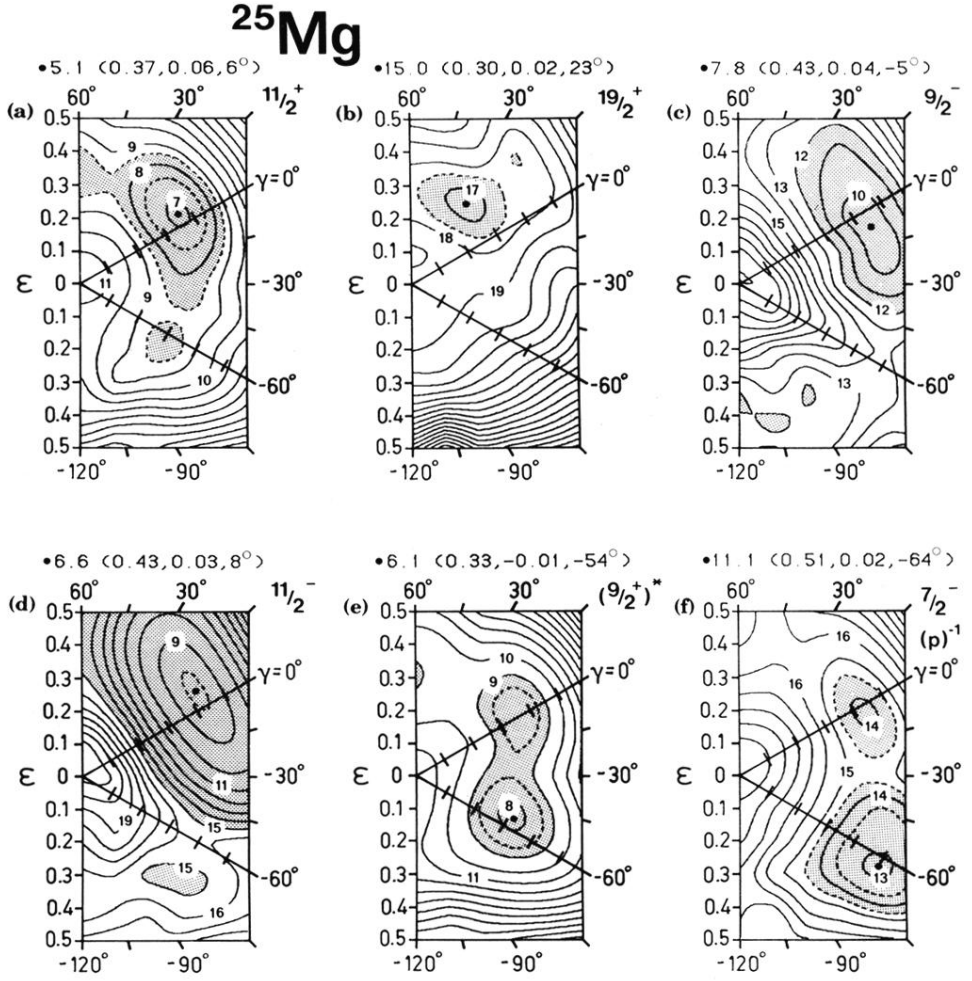


FIG. 14. Potential-energy surfaces in $^{25}$Mg as in Fig. 13. (a) and (b) $(\pi,\alpha)=(+,-\frac{1}{2})$ yrast configurations for $J=\frac{11}{2}$ and $\frac{19}{2}$. (c) and (d) Negative-parity yrast potential-energy surfaces for the $\nu(f_{7/2})$ configuration for $J=\frac{9}{2}$ and $\frac{11}{2}$. (e) $J=\frac{9}{2}$ surface for the one-hole configuration corresponding to $[211]\frac{3}{2}$ and $[200]\frac{1}{2}$ rotational bands, for prolate ($\gamma=0°$) and oblate ($\gamma=-60,$) deformations, respectively. (f) $J=\frac{7}{2}$ surface for the lowest-$p$-shell excitation in $^{25}$Mg.